Acceleration of the $d + d$ reaction in metal lithium acoustic cavitation with deuteron bombardment from 30 to 70 keV

Y. Toriyabe,[1,*] E. Yoshida,[1] J. Kasagi,[1,†] and M. Fukuhara[2]

[1]*Research Center for Electron Photon Science, Tohoku University, 1-2-1, Mikamine, Sendai 982-0826, Japan*

[2]*Institute for Materials Research, Tohoku University, Japan*

(Received 23 December 2011; published 24 May 2012; corrected 29 May 2012)

Fusion reactions ^{6}Li$(d,\alpha)^4$He and ^{2}H$(d,p)^3$H were measured in liquid Li. An ultrasonic target system was developed to form acoustic cavitation bubbles in liquid Li as an additional target. The material uncertainties of the target surface, which have been noted in solid target experiments, were completely rejected because contaminants could be removed in the liquid phase. The Li + d reaction was not affected by the cavitation process, and the derived screening potential was $U_s = 543 \pm 38$(sta.) $^{+83}_{-153}$(sys.) eV. This value can be explained by ionic Debye screening if liquid Li is regarded as a low-temperature dense plasma. The $d + d$ reaction was found to be enhanced several times by Li cavitation, whereas the yield of the Li + d reaction remained constant; the ultrasonic effect depends strongly on the target conditions. The enhancement is caused not by Coulomb screening but by the high deuteron temperature in the cavity. The temperature was deduced from the energy dependence of the nuclear reaction enhancement rate as $kT_d = 590 \pm 54$(sta.) $^{+676}_{-457}$(sys.) eV. A kinematic analysis also yielded consistent results. Although no meaningful bubble fusion events were observed, extremely large reaction enhancements were occasionally observed.

DOI: 10.1103/PhysRevC.85.054620 PACS number(s): 25.45.−z, 26.20.−f, 28.52.−s

I. INTRODUCTION

Low-energy nuclear reactions are of prime importance in nuclear syntheses and energy production in stars, where thermonuclear reactions occur under various plasma conditions [1]. In astrophysical plasmas, electrons screen the Coulomb barrier, enhancing the nuclear reaction rates by many orders of magnitude [2,3]. Hence, both cross sections of bare nuclei and estimation of the enhancement due to electron screening under stellar plasma conditions are essential.

The cross section of the interaction between bare nuclei, $\sigma_0(E)$, is expressed using the astrophysical factor $S(E)$ as

$$\sigma_0(E) = \frac{S(E)}{E} \exp[-2\pi\eta(E)], \tag{1}$$

where E is the energy in the center-of-mass system. The Sommerfeld parameter $\eta(E)$ is defined as $\eta(E) = \alpha Z_1 Z_2 \sqrt{\mu c^2/2E}$, where α, $Z_{1,2}$, μ, and c are the fine structure constant, atomic number of the interacting nuclei, reduced mass, and speed of light, respectively. Because of the Gamow factor, $\exp[-2\pi\eta(E)]$, the cross section drops steeply at energies far below the Coulomb barrier. When the screening effect is important, the cross section can be evaluated by introducing an effective energy difference U_s, which is generally called the screening potential. The generalized cross section $\sigma(E)$ can be expressed using the bare cross section $\sigma_0(E)$ as

$$\sigma(E) = \sigma_0(E + U_s) \tag{2}$$

$$= \frac{S(E + U_s)}{E + U_s} \exp[-2\pi\eta(E + U_s)], \tag{3}$$

where U_s is usually assumed to be an energy-independent constant. If the reaction enhancement is caused by only the electron screening effect, Eq. (2) should be replaced by $\sigma(E) = S(E)E^{-1} \exp[-2\pi\eta(E + U_s)]$.

In a laboratory, the S factor is usually measured by an accelerator beam experiment. This factor is parameterized from an excitation function as a function of E at relatively high energies and is extrapolated to lower energies. On the other hand, systematic measurements are impossible in gas plasmas. In stable gas plasma in the International Thermonuclear Experimental Reactor (ITER), the planned achievable density is $\sim 10^{14}$ cm^{-3}, which is much less than that in the Sun's core. Although a pinch plasma can provide densities of up to $\sim 10^{20}$ cm^{-3} [4], the confinement time is quite short.

The electron screening effect has been experimentally studied in gas and solid materials for the past 20 years [5,6]. In a solid metal environment, the density of conduction electrons is typically on the order of 10^{22} cm^{-3}. This environment can be regarded as a type of a low-temperature, high-density plasma. To date, the problem is that the experimentally reported values of U_s have been appreciably larger than theoretical predictions, especially in solid metals [7–11]. Furthermore, the screening potential depends strongly on the host material species. Although Raiola *et al.* proposed the application of the classical Debye screening model to quantum electrons in solid matter [9,10], the validity of this approach is still in dispute [11]. Thus, a deeper understanding of the role of the dense electron plasma is desirable.

In this paper, we describe the screening effect in a liquid metal Li environment. Using liquid metal as a host material is a natural extension in order to develop dense plasma environments for nuclear reactions for the following two reasons. First, large screening potentials were observed in metals at a low deuteron absorption ratio (low solubility), whereas the potentials were small in insulator materials,

*toriyabe@lns.tohoku.ac.jp
†kasagi@lns.tohoku.ac.jp

including gas targets. The correlation between the solubility and the screening potential implies that dynamic motion of the target enhances the reaction [7,9]. Second, the experiments reported to date have been conducted in the solid and gas phases, and no measurements have been performed in the liquid phase. The mobility of target particles is much higher than that in the solid phase; thus, a larger screening potential can be expected. Furthermore, no information on positive ions in experiments with solid metals is available despite the importance of electrons.

In liquid metal Li, all Li atoms are dissolved into Li^{1+} and e^-. The number densities of both positive ions and electrons are much higher than those in gas plasmas. Thus, liquid metals are regarded as strongly coupled plasmas in which the electron gas is degenerate, and classical ions undergo long-range correlation forces. The average interaction energy between the particles is larger than the average kinetic energy. Therefore, not only electrons but also ions can provide a screening effect; the well-known ionic Debye screening [12] can be expected. When we assume a Yukawa-type screening potential, the screened Coulomb potential $V_s(r)$ is expressed as

$$V_s(r) = \frac{1}{4\pi\epsilon_0}\frac{Z_1 Z_2 e^2}{r}\exp\left(-\frac{r}{\lambda_D}\right), \tag{4}$$

$$\sim \frac{1}{4\pi\epsilon_0}\frac{Z_1 Z_2 e^2}{r} - \frac{1}{4\pi\epsilon_0}\frac{Z_1 Z_2 e^2}{\lambda_D}, \tag{5}$$

where ϵ_0 is permittivity and the second term is assumed to be U_s. Here

$$\lambda_D = \sqrt{\frac{\epsilon_0 kT}{N_{\rm ion}(Q_{\rm ion}e)^2}} \tag{6}$$

is the screening length, where k, $N_{\rm ion}$, and $Q_{\rm ion}$ are the Boltzmann constant, ion number density, and ion charge number, respectively. Although Debye screening plays an important role in the kinetics of all components in aqueous solutions or plasmas, experiments that quantitatively or even qualitatively demonstrate Coulomb screening are rare. These predictions suggest that low-energy nuclear reactions are enhanced very strongly in a liquid metal target.

Taleyarkhan *et al*. reported another approach for providing high-density, high-temperature conditions in a table-top-size experiment. They examined $d + d$ nuclear fusion induced in acoustic cavitation generated by ultrasonic (US) waves in a liquid of deuterated acetone ($C_3{}^2H_6O$), which is called bubble fusion [13–15]. Similar experiments by other groups, however, have failed to confirm bubble fusion [16,17], and the occurrence of fusion through the cavitation process has been in dispute. It is commonly accepted that high temperature and high pressure are realized inside a bubble when the bubble collapses. Calculations have predicted the existence of a hot, optically opaque plasma core [18–20]. If the temperature exceeds 10^6 K, as some calculations have predicted, deuterium can undergo nuclear fusion. Although the existence of the plasma core and the lower limit of its temperature were published recently [21], no experimental evidence that quantitatively demonstrates a sufficiently high temperature for nuclear fusion has been reported. If the plasma core is optically opaque, the plasma temperature cannot be measured by optical methods.

To extend the plasma conditions for nuclear reactions that can be realized in a small experiment, we combined the two experimental concepts described above, i.e., low-energy nuclear reactions in liquid Li and US cavitation. A sophisticated liquid target chamber was constructed to achieve acoustic cavitation in liquid metal Li. In this paper, we report, for the first time, the ^{6}Li$(d,\alpha)^4$He and ^{2}H$(d,p)^3$H fusion reactions in liquid Li with/without acoustic cavitation during low-energy deuteron beam bombardment. Various conditions of the input US wave, target surface, and beam intensity were examined in order to observe the effects of the US wave and the material phase dependence. Bubble fusion events were also measured. The excitation functions were analyzed in terms of the screening energy and the temperature in the acoustic cavity.

One of the aims of the present study is to measure the $Li + d$ reaction in liquid Li and to discuss the enhanced screening effect in a low-temperature, high-density plasma. The other is to investigate the effect of acoustic cavitation on the $Li + d$ and $d + d$ reactions during deuteron bombardment and to ask whether high temperatures and the screening effect are realized. The next section describes the experimental details, in particular, those for the acoustic cavitation system. Since the conditions for achieving US cavitation in liquid Li are unknown, the results and a discussion of the survey measurements are given in Sec. III. To date, the effect of US cavitation has been seen only in the ^{2}H$(d,p)^3$H reaction. Thus, we deduce the screening energy of the ^{6}Li$(d,\alpha)^4$He reaction in liquid Li in Sec. IV. The effect of US cavitation on the ^{2}H$(d,p)^3$H reaction is described in Sec. V. Further discussion is presented in Sec. VI, and our results are summarized in Sec. VII.

II. EXPERIMENT

A. Ultrasonic system and lithium cavitation

A high-intensity acoustic field in liquid matter forms cavities or bubbles. The bubbles repeatedly expand and contract according to pressure oscillations of the US wave. The simplest example of bubble growth and collapse during the US cycles is shown in Fig. 1. A nucleus appears at low density; the bubble expands and contracts through several cycles and finally collapses at higher density. Since the speed of contraction approaches that of sound, the process proceeds adiabatically, producing high pressure, density, and temperature at the center of the cavity. Numerical simulations predicted shock wave formation in the cavity [22,23]. Atoms in the cavity are excited because of the high temperature and emit light, which is called sonoluminescence. Two types of acoustic cavitation and sonoluminescence are studied. One is a single-bubble system and single-bubble sonoluminescence (SBSL), in which a stably oscillating single bubble emits light in each compression phase [24]. The other is a multibubble system and multibubble sonoluminescence (MBSL), in which countless bubbles are generated, many of which emit light. Unless otherwise specified, "the acoustic cavitation" refers to the multibubble system in this paper.

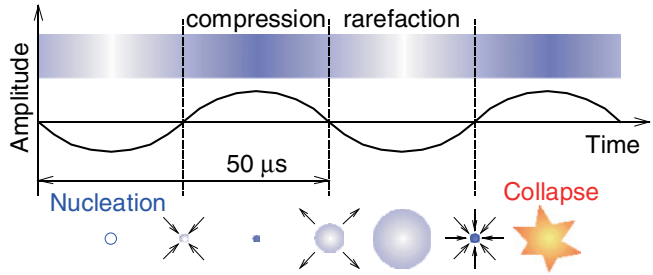

FIG. 1. (Color online) Bubble growth and collapse through US cycles. Bubble created at low density repeatedly expands and contracts, finally collapsing at higher density. High temperature and high pressure can be achieved at the center of the bubble. US wave frequency is about 20 kHz.

To prepare the Li acoustic cavitation target and bombard it with a low-energy deuteron beam, a vacuum chamber equipped with a US generator system was constructed. Figure 2 illustrates a schematic view of the US system; a plot of vibration amplitude versus position appears on the right. Note that the sonic waves are not transverse but longitudinal waves that form alternating conditions of density and rarefaction. A bolt-clamped Langevin-type transducer (BLT, Honda Electronics) placed at the bottom of the system generates a sonic wave. The BLT consists of four piezoelectric elements made of lead zirconate titanate (PZT). When the BLT is driven with an appropriate frequency, it outputs a high-amplitude wave because of resonance of the vibrations produced in the four piezoelectric elements. We designed the total length of the system such that the Li target position corresponds to an antinode under a resonant condition having a frequency of about 19 kHz. A horn made of Al connects the BLT and a liquid target holder. At the node position of the resonant sonic wave, the horn has a flange, where the US system is fixed with a vacuum chamber. Thus, the Li target can be placed in vacuum while the BLT is in air. The horn has an exponentially tapered shape that amplifies the vibration amplitude of the US wave by shrinking the diameter from 50 mm (bottom) to 23 mm (top). A Li holder (15 mm in diameter and 3.5 mm deep) made of stainless steel (SUS316L) is placed at the tip of the system. Sonic waves can pass vertically through the vacuum chamber wall with the minimum loss and reach the Li target.

Lithium is chemically so active that the surface is easily contaminated even in vacuum, where the primary residual gas is water vapor. Furthermore, carbon is steadily deposited on the beam spot during beam bombardment. These surface contaminants strongly affect the measurement results of the screening potential with a low-energy beam [11,25]. To obtain an accurate result, the Li surface should be kept completely clean. Therefore, the vacuum chamber contains essential tools to prepare clear liquid Li. A glove box is connected to the target chamber as its extended part. This structure makes it possible to handle the Li in a high-purity Ar atmosphere so it is never exposed to another gas until the end of the experiment. Since the glove box is evacuated by a turbomolecular pump, water vapor can be exhausted more effectively than by a gas

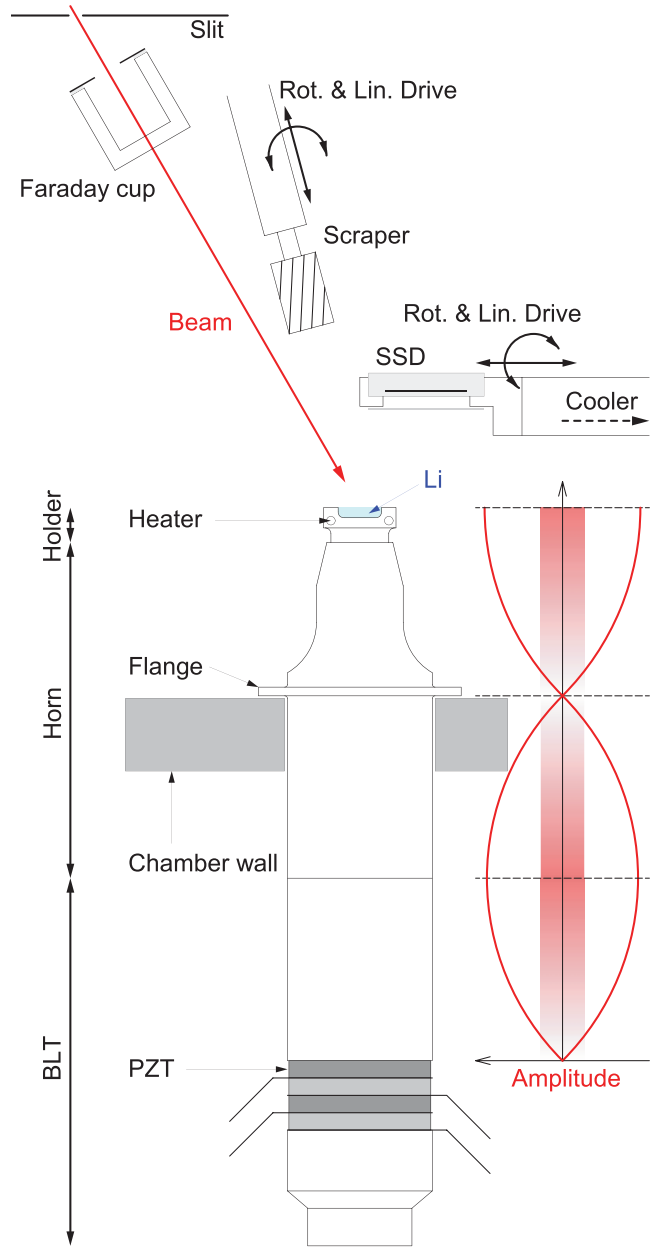

FIG. 2. (Color online) Schematic view of experimental setup. A BLT generates US waves, which are irradiated vertically to a Li target placed at the tip of the US system. Liquid Li target is 15 mm in diameter and 3.5 mm deep. Vibration amplitude is illustrated on the right at a resonance frequency of about 19 kHz. The US system was designed by matching the Li surface with the antinode position; the system is connected to a vacuum chamber at the node position to minimize losses. A scraper can remove contaminants floating on the liquid Li surface to maintain a completely clean surface. A cut beam 5 mm in diameter is injected at an angle of 60° with respect to the horizontal. A removable Faraday cup samples the beam current periodically. Charged particles are detected by an SSD, which has an active area of 600 mm^2, a thickness of 300 μm, and a 5-μm-thick Al absorber. The solid angle and detection angle are $\Omega/4\pi = 2.7\%$ and $\theta_{lab} = 124^\circ$ with respect to the beam direction, respectively. The SSD was cooled to 5 °C, where the typical energy resolution is about 200 keV in FWHM for 5.486-MeV α particles.

substitution procedure. After a sample of Li is cut and shaved for placement in the glove box, the Li target is transferred directly to the target chamber. The chamber then is evacuated to a pressure on the order of 10^{-5} Pa (typically 2×10^{-5} Pa).

The temperature of the Li target is controlled by ohmic heaters inserted in the holes of the holder and monitored by an infrared thermometer outside of the chamber. In the measurements, the temperature was maintained above 200 °C; the melting point of Li is 180 °C. Since the vapor pressure of Li below 300 °C is on the order of 10^{-6} Pa [26], evaporation was suppressed. When Li melts, impurities float on its liquid surface because their melting points are much higher than that of Li. The chamber contains a cleaning system that removes these impurities in vacuum. A scraper driven manually with linear and rotary motion feedthrough skims off the surface contaminants. After all of them are removed, a completely clear black surface is obtained. It is essential to avoid any erroneous analysis caused by unnoticed surface contaminants, as discussed for solid target experiments [11,25].

If the Li target is clean, countless bubbles cover the surface of the liquid Li under US operation; this is categorized as multibubble cavitation. The typical resonance frequency of the US system is 18.85 kHz. In this study, the targets of the incident deuterons are bubbles, so they should exist within the range of the deuterons, within a few micrometers. Furthermore, the liquid must be placed inside the vacuum chamber. Under these conditions, it is quite difficult to realize single-bubble cavitation, which may yield highly precise information on the state of the bubble; a single-bubble cavitation target will be considered in the future to obtain more precise data.

The Li surface is covered by contaminants again after several hours, and bubbles do not appear on the surface. The Li always reacts with residual gases in the chamber and microcracks in the holder; thus, contaminants accumulate and cavitation occurs below the contaminant layer. Since the layer is thicker than the incident deuteron range, deuterons lose energy within the contaminant layer before arriving at the cavitation sites. The reaction yield is strongly affected not only by the layer but also by even a small quantity of impurities, as described below. The cleanness of the Li surface is, therefore, a key factor in reaching correct conclusions. The surface cleaning process was repeated periodically during the experiment to keep the surface clear of impurities. However, target deterioration cannot be controlled, although it seems that it tends to be accelerated when the cavitation becomes intense with increasing vibration amplitude. We examined the target surface after each measurement, and the data acquired with a deteriorated surface were not employed.

B. Li + *d* and *d* + *d* measurements

We bombarded the Li target with a low-energy deuteron beam and measured the charged-particle emissions with a Si semiconductor detector (SSD). A low-energy ion generator provided deuteron beams at bombardment energies of 30 to 70 keV with an accuracy of ±50 eV. The beam was vertically bent by 60° with respect to the horizontal and injected into the target chamber from an upper port. Inside the chamber, a 5-mm-diameter aperture and a movable Faraday cup were aligned in front of the Li target. During the measurement, the beam's electric current was measured by inserting the Faraday cup for periodic sampling at a rate that was controlled by a data acquisition program. The amount of total charge bombardment was calculated from the sampled current value. The SSD has an active area of 600 mm^2 ($\Omega/4\pi = 2.7\%$) and a thickness of 300 μm; it was placed at an angle of $\theta_{lab} = 124$ °C with respect to the beam direction. The SSD was cooled to 5 °C to improve energy resolution. A 5-μm-thick Al foil covered the detector to stop elastically scattered deuterons, δ-ray electrons, and sputtered Li particles. The typical energy resolution for this setup is about 200 keV in full width at half maximum (FWHM) for 5.486-MeV α particles. The target was an isotopically enriched Li metal (95% ^{6}Li, 5% ^{7}Li, ISOTEC). In the experimental temperature range, the number density of the ^{6}Li in liquid phase is regarded as constant at $N_{^6\mathrm{Li}} = 4.42 \times 10^{22}$ atom/cm^3 [26–28].

A typical energy spectrum obtained with the liquid Li target is shown in Fig. 3. The highest energy peak corresponds to 11.2-MeV α particles from the ^{6}Li$(d,\alpha)^4$He reaction. Two nearby peaks around 4 MeV correspond protons from the ^{6}Li$(d,p_{0,1})^7$Li reactions. The continuous distributions of events below 7.5 MeV represent to α particles from the ^{7}Li$(d,\alpha)n^4$He reaction. The peak below 3 MeV corresponds to protons from the ^{2}H$(d,p)^3$H reaction. Here incident deuterons accumulate in liquid Li through beam bombardment and are regarded as additional targets. The ^{2}H$(d,p)^3$H reaction yield in liquid Li is a several orders of magnitude smaller than that in a solid metal target. The reason is that deuterons accumulate in interstitial metal ion sites in the solid target, whereas they move freely in the liquid target due to the lack of lattice structure.

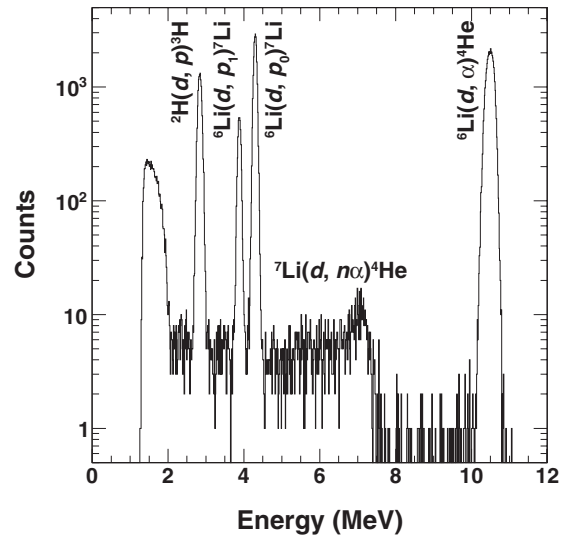

FIG. 3. Typical charged-particle energy spectrum observed with a clear liquid Li target bombarded with a deuteron beam (E_d = 50 keV). Detector is covered by a 5-μm-thick Al foil. Continuous component below 2 MeV consists of low-energy particles such as ^{2}H(d,t)H, ^{2}H$(d,{}^3\mathrm{He})n$, and ^{6}Li$(d,t\alpha)$H. Particles from secondary reactions such as (n,p) or (n,α) reactions are also included in the continuous events. Component below 1.5 MeV is discriminated.

TABLE I. Cycle of alternating data acquisition program.

	Time (s)							
	3	10	3	10	3	10	3	10
Beam	Off	On	Off	On	Off	On	Off	On
US	Off	Off	On	On	Off	Off	On	On

The number density of deuterons can be roughly estimated by the yield ratio between the ^{2}H$(d,p)^3$H and ^{6}Li$(d,\alpha)^4$He reactions. Under typical experimental conditions, it is less than 0.1% of the number density of ^{6}Li. The continuous component below 2 MeV represents low-energy particles such as ^{2}H(d,t)H, ^{2}H$(d,{}^3$He$)n$, and ^{6}Li$(d,t\alpha)$H. Particles from secondary reactions such as the (n,p) or (n,α) reactions are also included in the continuous events. In this study, we analyzed the two prominent peaks from the ^{6}Li$(d,\alpha)^4$He and ^{2}H$(d,p)^3$H reactions.

The yields in the US-on and -off states were compared to elucidate the US effect. However, the target condition was sensitive and readily deteriorated within several minutes because of the high activity of liquid Li, as described in Sec. II A. Therefore, we adopted an alternating data acquisition program in which the experimental conditions and the on/off states of the beam and the US wave were synchronized. This program switched the US wave off and on and measured the reaction yields in the US-on and -off states while minimizing the systematic errors. The data acquisition sequence is shown in Table I. The beam was repeatedly turned off for 3 s and on for 10 s, while the US wave was turned off and on every 13 s; hence, four data sets were accumulated in each cycle. Here "beam-off" means that the Faraday cup is inserted at the beam position and the target is not exposed to the deuteron beam. The average beam current during the beam-on state was interpolated as the mean value of the currents during the two beam-off states before and after the beam-on state.

Survey measurements performed under various experimental conditions showed that the reaction yield also depends strongly on the target condition, as described in Sec. III A. Thus, the data analyzed in the present study were those accumulated under relatively stable conditions. The beam and target conditions for the measurements are summarized in Table II.

TABLE II. Experimental conditions. Ultrasonic effects were surveyed under many experimental conditions. When the energy dependence of the reaction yields was measured precisely, the parameters were fixed at a relatively stable condition.

Parameters	Survey	Precise
Beam energy, E_d (keV)	25–70	30–70
Beam current, I (μA)	7–40	7–17
Beam input (mW)	200–2000	500
Li temperature, T (°C)	180–250	190–210
Vibration amplitude, P (μm)	1.8–5.0	1.9
Vacuum (Pa)	2×10^{-5}–1×10^{-3}	3×10^{-5}

III. DEUTERON BOMBARDMENT OF LIQUID LI WITH US CAVITATION

A. Reaction enhancement

The reaction yields of ^{6}Li$(d,\alpha)^4$He and ^{2}H$(d,p)^3$H as a function of the elapsed time are shown in Figs. 4(a) and 4(b), respectively. No impurities were found on the Li target surface after the measurements. The yield is defined as the number of counts for the ^{6}Li$(d,\alpha)^4$He or ^{2}H$(d,p)^3$H reaction normalized by the electric charge, which is equivalent to the number of incident deuterons. Since the yields were measured alternately in the US-off and -on states, as described in Sec. II B, the data points obtained under each condition are plotted in turn. As shown in Fig. 4(a), the average yields for the $\mathrm{Li} + d$ reaction in the US-off and -on states are 0.675 ± 0.014 (dotted line) and 0.668 ± 0.012 counts/μC (solid line), respectively. The values overlap each other within the error, and no significant US effect was observed. In contrast, the yield of the $d + d$ reaction for the US-on state is always higher than that for the US-off state, as shown in Fig. 4(b). The averages are 0.109 ± 0.006 and 0.153 ± 0.007 for the US-off and -on states, respectively. Overall, the US effect causes a 40% yield increase with a reliability of 3.4σ. To see the time dependence more clearly, the US-on/-off yield ratios (ratios of the yield in the US-on state to that in the US-off state) for both reactions are plotted in Fig. 4(c). The data points for the $d + d$ reaction consistently exceed unity, whereas those for the $\mathrm{Li} + d$ reaction remain around unity. The average yield ratios are 0.99 ± 0.02 (dotted line) and 1.40 ± 0.10 (solid line) for the $\mathrm{Li} + d$ and $d + d$ reactions, respectively. As described below, the target density in the US-on and US-off states remains at almost the same level. The reaction is enhanced not by a change in the target density but by an increase in the cross section. By examining many other measurements, we obtained qualitative information about the US effect. A lack of enhancement in the $\mathrm{Li} + d$ reaction with a notable enhancement in the $d + d$ reaction is a common feature of US operation with a clean surface.

When the Li surface was covered with contaminants and bubbles ceased to appear, no such reaction enhancement was observed. Figures 4(d)–4(f) show the same type of information as in Figs. 4(a)–4(c) but for a dirty target. Since the surface was completely covered with a contaminant layer, the target was not pure Li liquid but a solid Li compound phase. As shown in Fig. 4(d), the yields for the $\mathrm{Li} + d$ reaction in both US-off and -on states remained almost constant at around the average values shown in Fig. 4(a). For the $d+d$ reaction, however, both yields increased steeply with the elapsed time, as shown in Fig. 4(e). Because the surface gets covered with a contaminant layer during bombardment, the spot where the $d + d$ reaction occurs changes gradually from the liquid Li phase to the solid Li compound one. Deuterons accumulate easily in the solid contaminated target, so the target deuteron density increases as the elapsed time increases. In the solid phase, no US effect seems to exist. This is seen more clearly in Fig. 4(f), which shows the US-on/-off yield ratio; the averages for the $\mathrm{Li} + d$ and $d + d$ reactions are 0.98 ± 0.02 and 0.98 ± 0.03, respectively. No significant enhancement was observed with the contaminated Li target. Therefore, the enhancement is caused not by the US wave itself but by the emergence of cavitation in liquid Li.

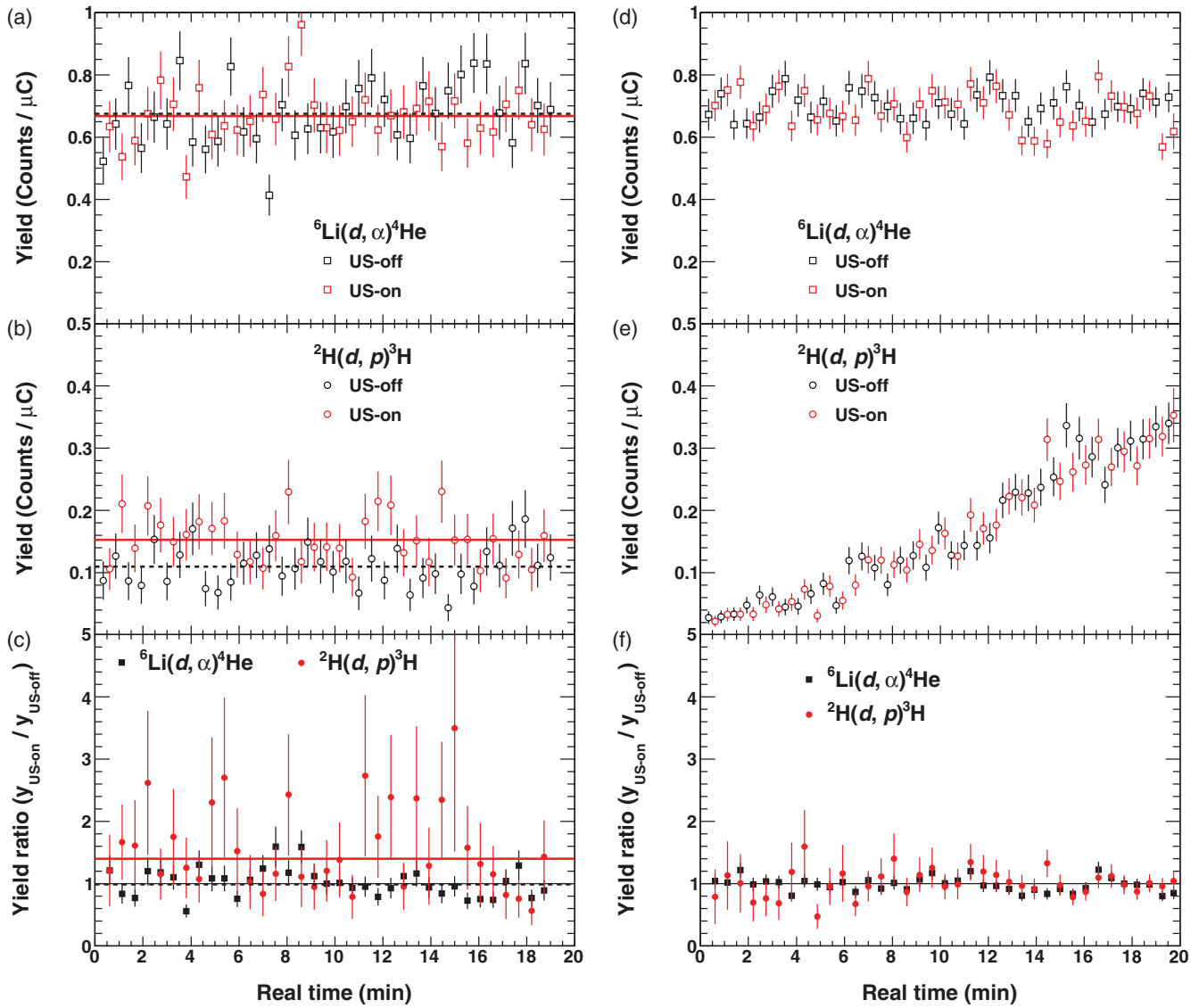

FIG. 4. (Color online) Typical reaction yields of [(a) and (d)] Li + d reaction, [(b) and (e)] $d + d$ reaction and [(c) and (f)] US-on/-off yield ratio as a function of elapsed time. [(a)–(c)] No impurities were found on the Li surface after the measurement. Vibration amplitude, beam energy, beam current, and temperature were $P = 1.9$ μm, $E_d = 50$ keV, $I = 9.3$ μA, and $T \sim 215$°C, respectively. (b) Yields in the US-on state are significantly higher than those in the US-off state for the $d + d$ reaction. Average values are (a) 0.675 ± 0.014 (dashed line) and 0.668 ± 0.012 (solid line) counts/μC for US-off and -on states, (b) 0.109 ± 0.006 (dashed) and 0.153 ± 0.007 (solid) count/μC for US-off and -on states, and (c) 0.99 ± 0.02 (dashed) and 1.40 ± 0.10 (solid) for Li + d and $d + d$ reactions, respectively. [(d)–(f)] Li was covered by a contaminant layer. Vibration amplitude, beam energy, beam current, and temperature were $P = 2.3$ μm, $E_d = 50$ keV, $I = 26.8$ μA, and $T \sim 215$°C, respectively. (e) Since deuterons diffused very little in the solid contaminant layer, the target deuteron density and, consequently, the yield, increased with the beam bombardment time. Average values are (d) 0.702 ± 0.008 and 0.687 ± 0.008 count/μC for US-off and -on states and (f) 0.98 ± 0.02 and 0.98 ± 0.03 for the Li + d and $d + d$ reactions, respectively.

Although we attempted over a hundred times to produce the conditions necessary for a greater US effect for a clean target surface, the measured values of the US-on/-off yield ratio were not reproduced very well. In Fig. 5, we summarize the results of these measurements under the same experimental conditions ($E_d = 50$ keV). The US-on/-off yield ratios of the Li + d reaction (α yield ratio) and the $d + d$ reaction (proton yield ratio) are plotted.

Although the proton yield ratio always exceeds 1.0, the values are very widely scattered up to 1.9. On the other hand, those of the α yield ratio are distributed much more narrowly, 1.0 ± 0.1. The enhancement of the $d + d$ reaction exhibits no correlation with that of the Li + d reaction. The enhanced reaction due to the US effect is seen only for the $d + d$ reaction, but the magnitude of the enhancement is not reproduced quantitatively in the present study. This is due to fluctuations in the sensitive target conditions rather than statistical errors.

The US-on/-off yield ratio for the $d + d$ reaction depended on the input US power, as shown in Fig. 6, where the ratios

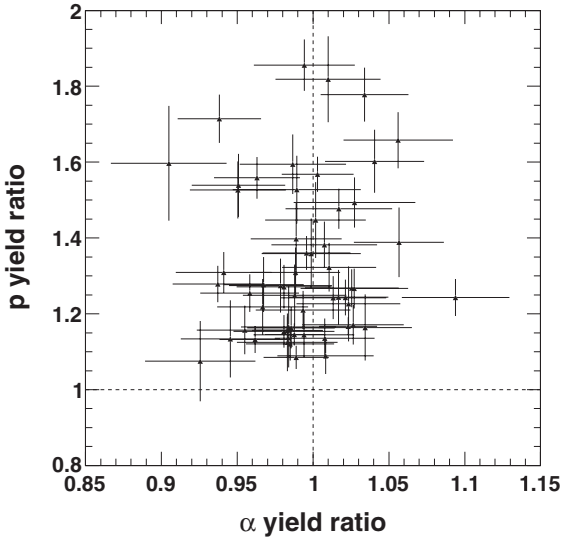

FIG. 5. Relationship between the US-on/-off yield ratios of the Li + d (α yield ratio) and $d + d$ (p yield ratio) reactions. Vibration amplitude and beam energy were $P = 1.9$ μm and $E_d = 50$ keV, respectively. Although all points exceed unity for the $d + d$ reaction, they are widely scattered because of the sensitive target conditions. Enhancement of the $d + d$ reaction exhibits no correlation with that of the Li + d reaction.

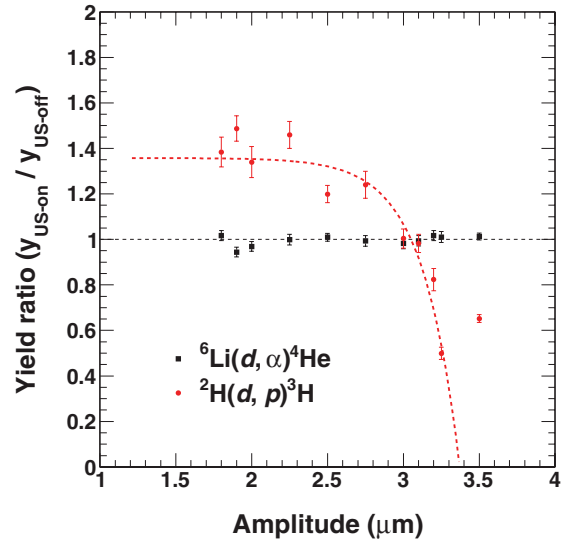

FIG. 6. (Color online) Vibration amplitude dependence of the US-on/-off yield ratios. Beam energy, beam current, and temperature were $E_d = 50$ keV, $I = 15$ μA, and $T \sim 220$°C, respectively. The yield ratio of the $d + d$ reaction tends to decrease with increasing amplitude, whereas the ratio of the Li + d reaction remains constant. Since intense US waves stir liquid Li, target deuterons are diffused away. The target density and, consequently, the reaction yield decrease in the US-on state. When the amplitude is further increased, for example, to 3.5 μm, the Li target is contaminated within a few minutes, and the ratio tends to recover to unity.

are plotted against the maximum displacement (vibration amplitude) at the target's surface. The data were accumulated in a chain of measurements, and special care was taken to maintain similar target conditions of $E_d = 50$ keV, $I = 15$ μA, and $T = 220$ °C. As expected, the yield ratios of the Li + d reaction are almost unity, and no significant enhancement is observed. On the other hand, the ratio of the $d + d$ reaction depends strongly on the vibration amplitude. The enhanced reactions appear only at lower amplitudes. The US-on/-off yield ratio seems to decrease suddenly for amplitudes above 2.8 μm and drops below unity at amplitudes above 3.0 μm. This behavior is unexpected because careful observation showed that cavitation clearly became violent as the vibration amplitude increased. At such a high amplitude, liquid Li is strongly stirred; hence, deuterons in the Li diffuse away. This reduces the target deuteron density; thus, the proton yield drops below unity. The reaction enhancement caused by the US-on state seems to be more effective than the reduction in the target density at lower amplitudes; consequently, the US-on/-off yield ratio exceeded unity. Note that the yield ratio of the $d + d$ reaction recovers at amplitudes greater than 3.5 μm. Under such a high vibration amplitude condition, the Li surface is covered with contaminants within several minutes. The target then changes from liquid Li to the solid contaminant layer, and cavitation can no longer be generated at the surface. Therefore, the US effect disappears, and the US-on/-off yield ratio is asymptotic to unity.

B. Strong enhancement

As described above, the target conditions change instantaneously and are uncontrollable. The US-on/-off yield ratio for the $d + d$ reaction is widely distributed even under the same conditions. In this study, the reaction yields have been measured under various experimental conditions, and strong enhancement (yield ratios greater than 2.0) has rarely been observed. For the strongest enhancement, the time-averaged US-on/-off yield ratio of the $d + d$ reaction became greater than 5, whereas that of the Li + d reaction remained at around unity. The energy spectra for the US-off and -on states for that run are shown in Figs. 7(a) and 7(b), respectively. The peak of the ^{2}H$(d,p)^3$H reaction for the US-on state is much higher than that for the US-off state. No significant enhancement was observed for the ^{6}Li$(d,\alpha)^4$He and ^{6}Li$(d,p_{0,1})^7$Li reactions in this run. The width of each peak in the US-on state is not clearly spread compared to those in the US-off state except the ^{2}H$(d,p)^3$H reaction as described below. The number of background events in the US-on state did not increase. These results indicate that electric and mechanical noise are not induced by US vibration.

The yields of the Li + d and $d + d$ reactions are plotted against the elapsed time in Figs. 7(c) and 7(d), respectively. For the Li + d reaction, the yields for both states are equivalent and constant. The average value is consistent with that obtained at the same deuteron energy, $E_d = 50$ keV, as shown in Figs. 4(a) and 4(d). For the $d + d$ reaction, the yield for the US-on state is several times larger than that for the US-off state. Since the yield in the US-off state remains almost constant, similarly to the case in Fig. 4(b), the target deuteron density can be regarded as constant during the measurement. The yield for the US-on state is particularly large for the first 5 min and

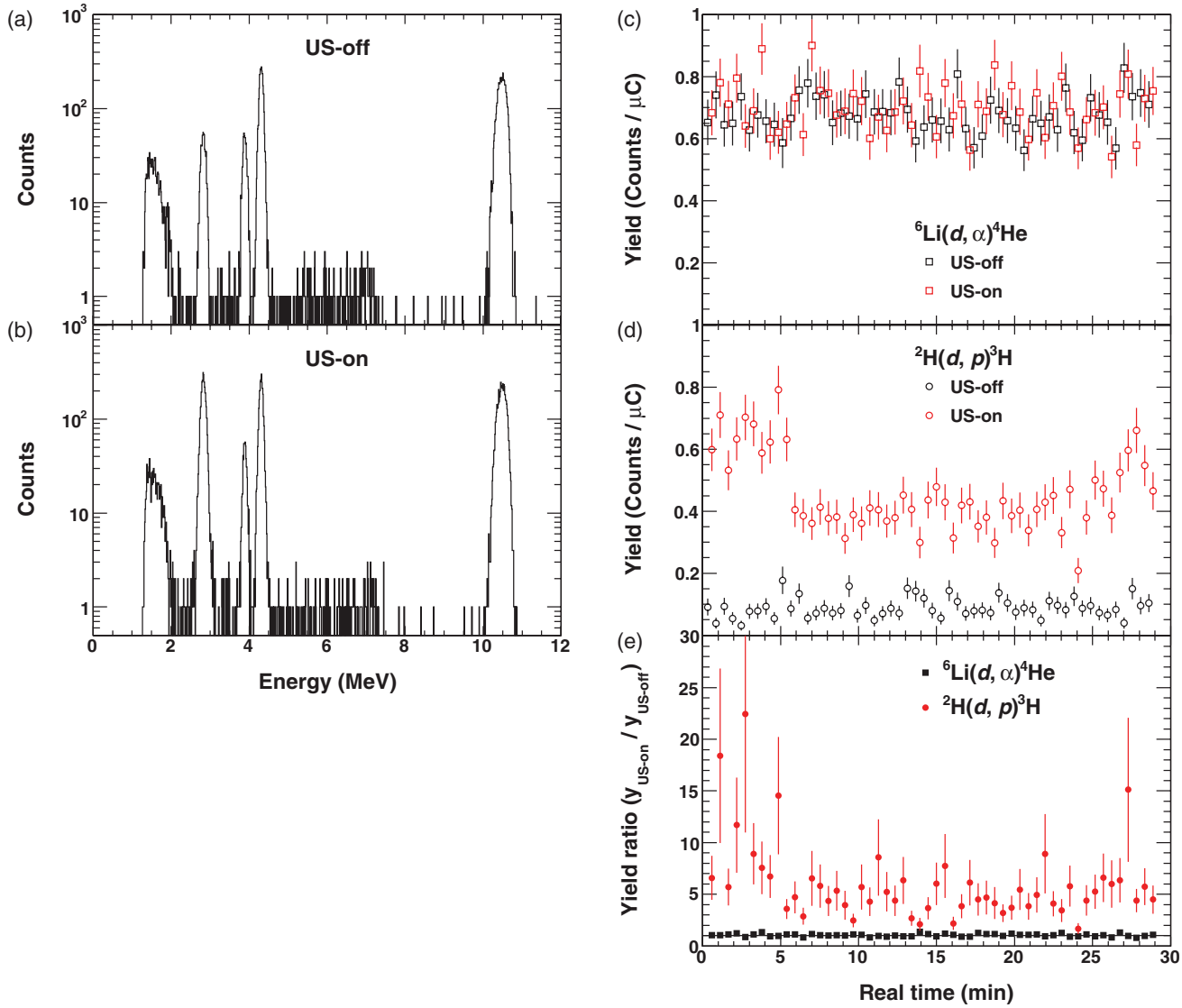

FIG. 7. (Color online) Energy spectra, reaction yields, and US-on/-off yield ratios as a function of elapsed time for the most strongly enhanced run. Vibration amplitude, beam energy, beam current, and temperature were $P = 1.9\ \mu$m, $E_d = 50$ keV, $I = 13\ \mu$A, and $T \sim 210^\circ$C, respectively. (a) Energy spectrum in the US-off state. Center of peak position of the ^{2}H$(d,p)^3$H reaction is 2824.2 ± 2.5 keV. (b) Energy spectrum in the US-on state. Peak count of the ^{2}H$(d,p)^3$H reaction is much larger than that in the US-off state. Center of peak is 2828.0 ± 1.1 keV. Peak position is shifted to higher energy and its width is spread slightly compared to that in (a). (c) Li + d reaction yields. Absolute values of the yields are constant and equivalent to those in Figs. 4(a) and 4(d). (d) $d + d$ reaction yields. The yields in the US-on state are much higher than those in the US-off state, especially in the first 5 min. The target condition changed at around 5 min owing to the instability of the Li cavitation target. (e) US-on/-off yield ratio for the Li + d and $d + d$ reactions. Average values are 1.03 ± 0.02 and 5.14 ± 0.23 for the Li + d and $d + d$ reactions, respectively. Note that the scales of the vertical axes in (d) and (e) differ from those in Figs. 4(b) and 4(e) and Figs. 4(c) and 4(f), respectively.

then drops abruptly by about 40%. This indicates the difficulty in maintaining long-term stability in the US cavitation target. The US-on/-off yield ratios are shown in Fig. 7(e); the time-averaged values are 1.03 ± 0.02 and 5.14 ± 0.23 for the Li + d and $d + d$ reactions, respectively. The instantaneous ratios exceeded 10.0 on several occasions. The corresponding events cannot be caused by statistical fluctuations or electrical noise.

Note that the peak of the ^{2}H$(d,p)^3$H reaction in Fig. 7(b) has two peculiar features: the peak shift and the width of the peak. The centers of the peaks for the US-off and -on states are at 2824.2 ± 2.5 and 2828.0 ± 1.1 keV, respectively. The peak in the US-on state is shifted to higher energy by about 4 keV, which is equivalent to a deviation of about 1σ. Furthermore, the foot of the peak in the US-on state spreads slightly toward higher energy. Spectra with an expanded scale are shown in Fig. 8(a) in order to display the second characteristic more clearly. The spectrum in the US-on state is the same as that in Fig. 7(b). That in the US-off state, however, is a summation of three data sets: the data shown in Fig. 7(a) and those taken just before and after the run. All the data were taken under the same

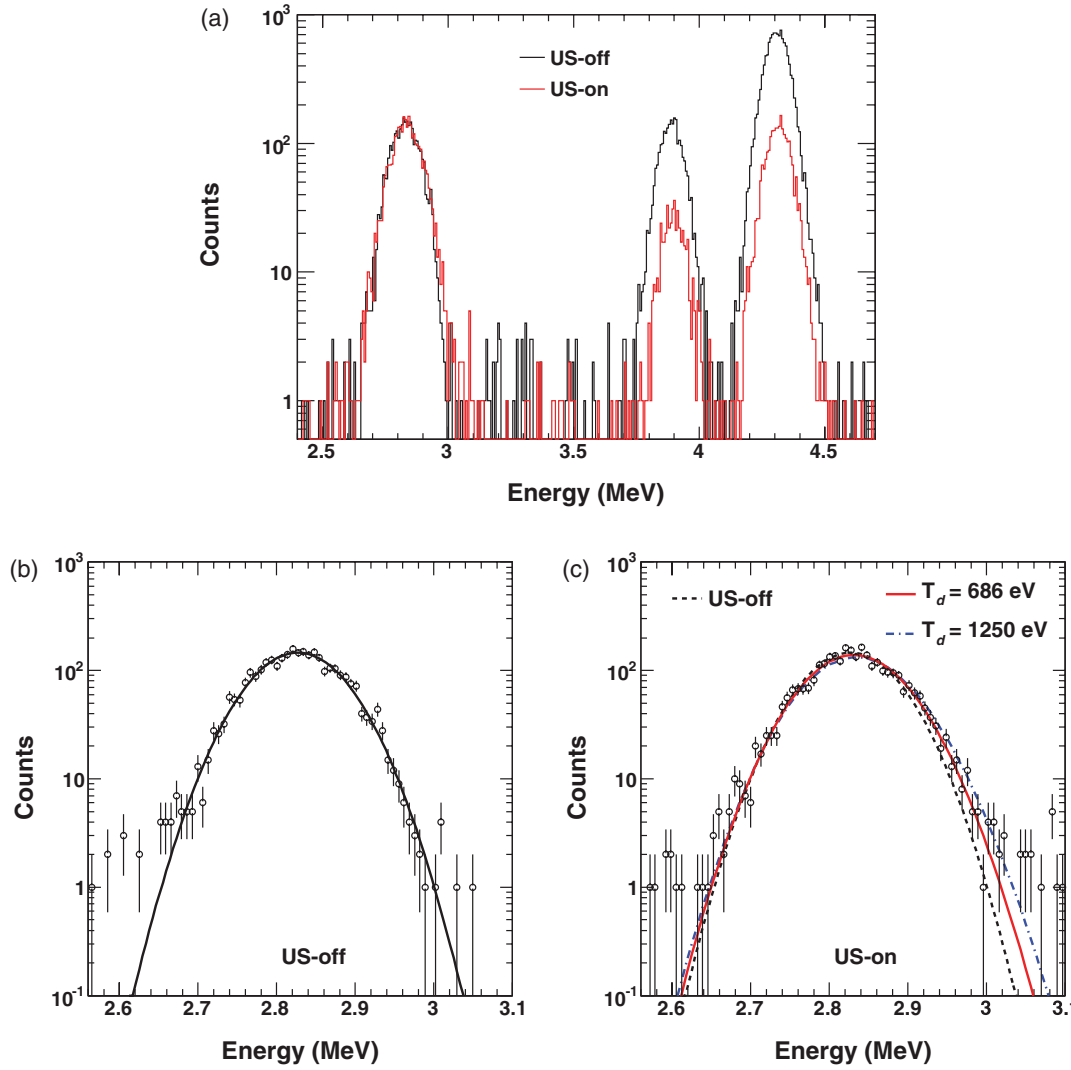

FIG. 8. (Color online) Energy spectra of the most strongly enhanced run at expanded scales. Data for the US-on state are exactly the same as in Fig. 7(b). Those for the US-off state are a summation of three data: those shown in Fig. 7(a) and those taken just before and just after that measurement. All the data were taken under the same experimental conditions. The total counts of both ^{2}H$(d,p)^3$H reaction peaks are adjusted to be the same. Background events in the US-off spectrum are subtracted randomly to obtain a level equivalent to those in the US-on state. (b) Detail of the ^{2}H$(d,p)^3$H peak in the US-off state. Data are the same as in (a). Solid line is a fitting result with reduced $\chi^2 = 1.242$. (c) Detail of the ^{2}H$(d,p)^3$H peak in the US-on state. Data and dashed line represent the same data as in (a) and a function shown in (b), respectively. Experimental plots are higher than the dashed line at the higher energy tail from 2.9 to 3.1 MeV. Solid and long dashed-dotted lines are numerically simulated spectra at target deuteron temperatures of $kT_d = 686$ and 1250 eV, respectively. Reduced χ^2 values are 1.721, 1.208, and 1.538 for $kT_d = 0$ (US-off), 686 eV, and 1250 eV, respectively. Percentage of gas phase is assumed to be 65% (liquid phase is 35%).

experimental conditions. The total counts for the ^{2}H$(d,p)^3$H reaction peaks are adjusted to those for the US-on state so as to compare the peak structure using the same statistics. Because the measurement duration becomes longer than that for the US-on state because of the summation, the number of counts of background events, such as the ^{7}Li$(d,\alpha)n^4$He, (n,p), and (n,α) reactions, also increased. Thus, the background events were subtracted randomly to obtain a level equivalent to those for the US-on state.

The ^{2}H$(d,p)^3$H peaks in the US-off and -on states in Fig. 8(a) are shown in detail in Figs. 8(b) and 8(c), respectively, at expanded scales. In Fig. 8(b), the solid line shows a fitting result, which agrees with the data well (reduced $\chi^2 = 1.242$). This function is also illustrated as a dashed line in Fig. 8(c). The dashed line, however, cannot replicate the higher energy tail, where the data points are higher than the function. This salient feature is observed only in the ^{2}H$(d,p)^3$H peak. For the other reactions, namely ^{6}Li$(d,p_{0,1})^7$Li and ^{6}Li$(d,\alpha)^4$He, no significant change in the peak structure or reaction enhancement was observed. The deformation of the spectrum can be regarded as a kinematic effect. The target deuteron has a meaningful momentum; in other words, the deuteron temperature in the cavity is meaningfully high. If the target deuteron moves rapidly enough and collides with the incident deuteron head-on, the reaction cross section increases dramatically and the energy of detected protons increases.

Numerically simulated spectra for deuteron temperatures of $kT_d = 686$ and 1250 eV are denoted in Fig. 8(c) by solid and long dashed-dotted lines, respectively. The high-energy tails tend to become large with increasing target deuteron temperature. Here we assume that the percentage of the gas phase at the liquid Li surface is 65% (liquid phase is 35%) on the basis of the discussion in Sec. V. The best fit is obtained at a deuteron temperature of $kT_d = 686 \pm 115$ eV or 7.96×10^6 K. The reduced χ^2 improves from 1.721 to 1.208 as kT_d increases from 0 (US-off) to 686 eV. The kinematically shifted spectrum can explain the experimental plot. Hence, the deuteron temperature in the cavity reaches at least on the order of 10^6 K in the most enhanced run. Furthermore, the above discussion indicates that the temperature in the cavity can be estimated by a kinematic analysis. We discuss the contradictory findings that the temperature of Li in the cavity is not high and no reaction enhancement was observed in Sec. VI.

C. Infrared thermometer readout

We found that the uncontrollable IR thermometer readout, qualitatively correlated with the reaction enhancement. Figure 9 shows the IR thermometer readouts as a function of elapsed time. The lines increase and decrease periodically in synchrony with the US-on/-off cycle. When the US waves were turned on, the IR thermometer readout increased immediately; it also decreased back to the initial value at the instant the US waves were turned off. The height of the steps, i.e., the differences between high and low temperatures, is positively correlated with the US-on/-off yield ratio. The temperature difference seems to increase with the yield ratio. Examples are shown in Figs. 9(a) and 9(b); the corresponding yield ratios were 1.38 ± 0.09 and 2.30 ± 0.09, respectively. Much larger differences in the apparent temperature appear in Fig. 9(b). Note that the periodic steps of the readout disappeared completely because of the absence of cavitation when the Li surface was covered with impurities. Although the reason for the fluctuation is unknown, it is not plausible that the change in the readout corresponds to a true temperature change because the response was instantaneous. One possible candidate for explaining the above characteristic is near-infrared radiation arising from Li cavitation as sonoluminescence.

D. Time correlation

The enhanced events due to the US effect are expected to exhibit a periodic time structure in this experiment. Since cavitation occurs on a periodic cycle, as shown in Fig. 1, the US effect should also be time dependent. In SBSL, for example, the cavity collapses periodically at a specific point in the US cycle [22–24]. The temperature in the cavity increases dramatically and reaches a maximum when the cavity contracts and collapses. In bubble fusion experiments, Taleyarkhan *et al.* reported a clear time structure of the neutron and γ-ray emissions, which are synchronized with the US cycle [29]. We conducted two time structure analyses for the Li + d and $d + d$ reactions in terms of micro and macro time sequences.

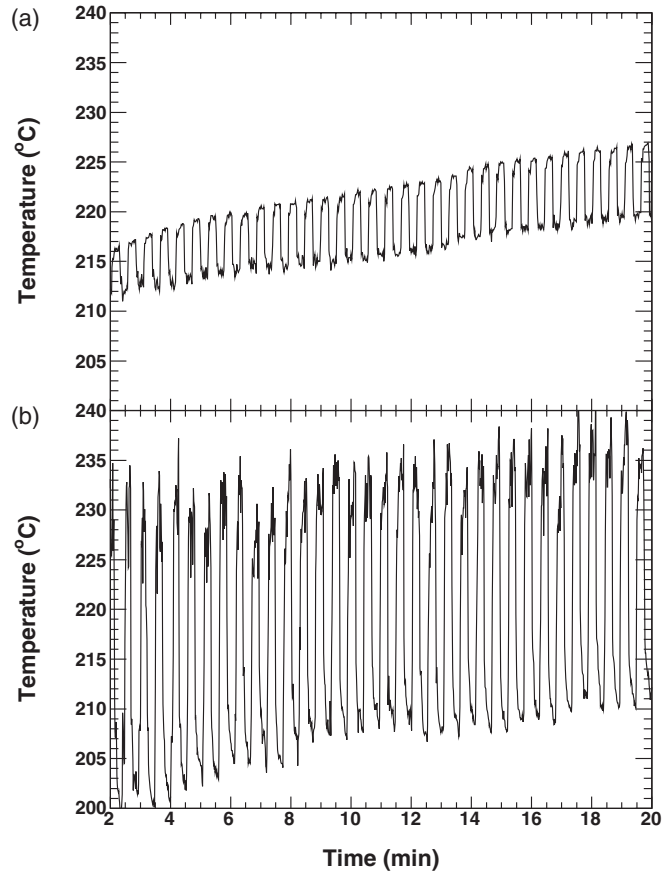

FIG. 9. Typical IR thermometer readouts in obviously enhanced runs. Output increases and returns to the initial value periodically in synchrony with the US on and off timing, respectively. The width of the fluctuation is positively correlated with the US-on/-off yield ratio; the average ratios are (a) 1.38 ± 0.09 and (b) 2.30 ± 0.09. Vibration amplitude, beam energy, and beam current were $P = 1.9$ μm, $E_d =$ 50 keV, and $I = 13$ μA, respectively.

The first is a micro time sequence that reflects the information within one cycle of the US wave. The US frequency is about 18.85 kHz; thus, one cycle is about 53 μs. Standard time signals were obtained from the US power supply when the vibration amplitude crossed a certain value, namely the discriminator level. Next, the time differences between each event signal and the nearest former standard signal were measured. Time spectra of a typical strongly enhanced reaction are shown in Fig. 10. The horizontal axis corresponds to the time difference between the standard signal and the event signal. In this case, the US-on/-off yield ratios were 0.96 ± 0.03 and 3.52 ± 0.10 for the Li + d and $d + d$ reactions, respectively, when the incident energy was $E_d = 40$ keV. Figures 10(a) and 10(b) show the spectra for the Li + d reaction in the US-off and -on states, respectively. No prominent structure appears in either histogram, and the average values are almost the same because no reaction enhancement was observed for the Li + d reaction. Although strong reaction enhancement was observed for the $d + d$ reaction, no meaningful time information was observed, as shown in Figs. 10(c) and 10(d). The histogram in the US-off state [Fig. 10(c)] is almost flat

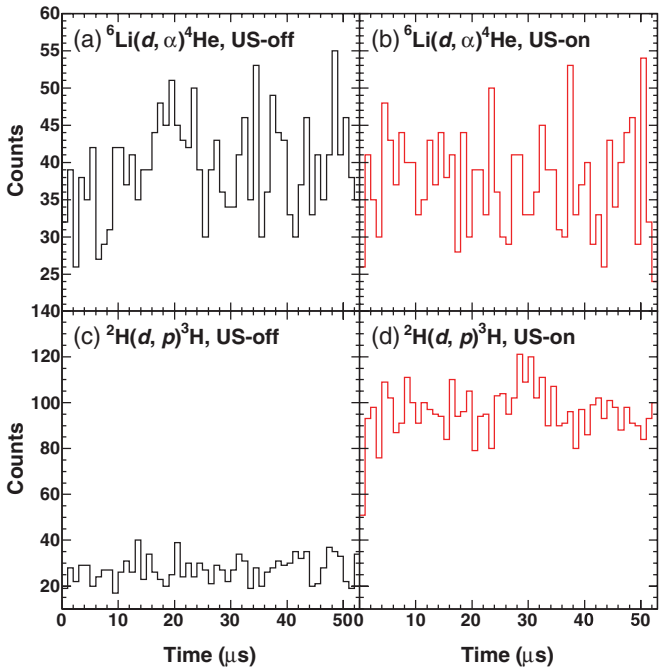

FIG. 10. (Color online) Micro time sequence information for the Li + d reaction in the (a) US-off and (b) US-on states and the $d + d$ reaction in the (c) US-off and (d) US-on states. Vibration amplitude, beam energy, beam current, and temperature were $P = 1.9\ \mu$m, $E_d =$ 40 keV, $I = 13\ \mu$A, and $T \sim 200\,^{\circ}$C, respectively. US-on/-off yield ratios of Li + d and $d + d$ reactions are 0.96 ± 0.03 and 3.52 ± 0.10, respectively. Horizontal axis corresponds to time difference between each event and the nearest former time standard signal. The two sequences are equivalent for the Li + d reaction because no US effect was observed. Although the number of counts for the $d + d$ reaction in the US-on state is much larger than that in the US-off state due to the strong enhancement, no meaningful peak structure appears.

because the reaction rate is constant and not time dependent. In the US-on state [Fig. 10(d)], prominent structure is also absent, except that the event counts are much larger than those in Fig. 10(c). A small bumplike structure around 30 μs is due to statistical fluctuations. If the reaction enhancement is correlated with bubble collapse, the histogram is expected to have a peak structure when the US waves compress the bubble. However, the sequence information for the US-on state shown in Fig. 10(d) exhibits no peak structure and no observable time correlation between the events and the US cycle. This means that enhanced $d + d$ reactions occur consistently in one cycle of the US wave.

The obtained results do not agree with the simple prediction discussed above. One might interpret this as indicating that the deuteron density near the beam spot increases due to US operation. This interpretation, however, contradicts the other results. The enhancement disappears at higher amplitudes, as shown in Fig. 6. Moreover, the US-on/-off yield ratio tends to have an incident energy dependence, which is described below. An increase in the deuteron density is expected to increase the US-on/-off yield ratio by a constant factor independent of the incident energy. Therefore, instead of a deuteron density change, the following explanation is more reasonable. The cavitation process is very complex, and a simple model can be applied only to limited cases such as the single-bubble system. Because the intensity of the US waves is strong, the bubbles become numerous in this experiment. Consequently, interactions between multiple bubbles affect the bubble growth cycle and the timing of the bubble collapses; the temperature becomes highest. The bubbles collapse at any time in the US wave cycle. Therefore, an enhanced reaction having no temporal correlation with the US cycle is observed.

In this study, meaningful micro time sequence information has never been obtained. In contrast, the macro time sequence information exhibited a structure when the reaction was sufficiently enhanced. To examine the time correlation between two successive events, the estimated spectra are shown in Fig. 11. The data are the same as those analyzed in Fig. 10. The horizontal axis corresponds to a time interval between an event and the next event, that is, between two events detected successively in the same reaction; the Li + d/Li + d and $d + d$/$d + d$ reaction intervals are shown in Figs. 11(a) and 11(b), respectively. A unique structure appears for the $d + d$ reaction in the US-on state, whereas the others have a common structure. We analyzed these histograms using predictions based on the Poisson process because nuclear reactions are modeled well with that process. This process, which is characterized by the constant rate parameter λ_0 and probability of occurrence k within the time interval t, is described as

$$P(N_t = k, t) = \frac{(\lambda_0 t)^k}{k!} e^{-\lambda_0 t}. \tag{7}$$

Thus, the distribution of the time interval between consecutive events, i.e., the interarrival time τ, is proportional to $e^{-\lambda_0 \tau}$. Here the constant λ_0 is equivalent to the reaction rate in the present analysis. The time correlation spectrum is expected to decrease exponentially with increasing event time interval at a constant reaction rate. In fact, the two spectra for the Li + d reaction shown in Fig. 11(a) are reproduced well by the function

$$y = I e^{-\lambda_0 t}, \tag{8}$$

where I is a constant. The fitting results are shown in Fig. 11(a); the derived values λ_0 for the US-off and -on states are $\lambda_0 = 1.09 \pm 0.04$ and 1.13 ± 0.05, respectively. These two derived reaction rates agree with not only each other but also the respective reaction rates within the experimental errors.

In Fig. 11(b), the spectrum for the US-off state can be fitted by the same function; the derived rate parameter is $\lambda_0 = 0.75 \pm 0.05$. However, the same analysis cannot be applied to that for the US-on state, which clearly has three components: (1) a straight component that is almost parallel to the US-off spectrum for $1.5 < t < 3.5$ s, (2) a steep component for $0 < t < 0.2$ s, and (3) a shoulder for $0.2 < t < 1$ s. The second component can be approximated by a straight line with a steep slope (large λ_0) which indicates a high reaction rate. Here components (1) and (2) might be regarded as originating from two Poisson processes with different λ_0 values. This interpretation, however, is inconsistent with the following property. Two independent Poisson processes $X(t)$ and $Y(t)$ with rate parameters λ_X and λ_Y yield a new process

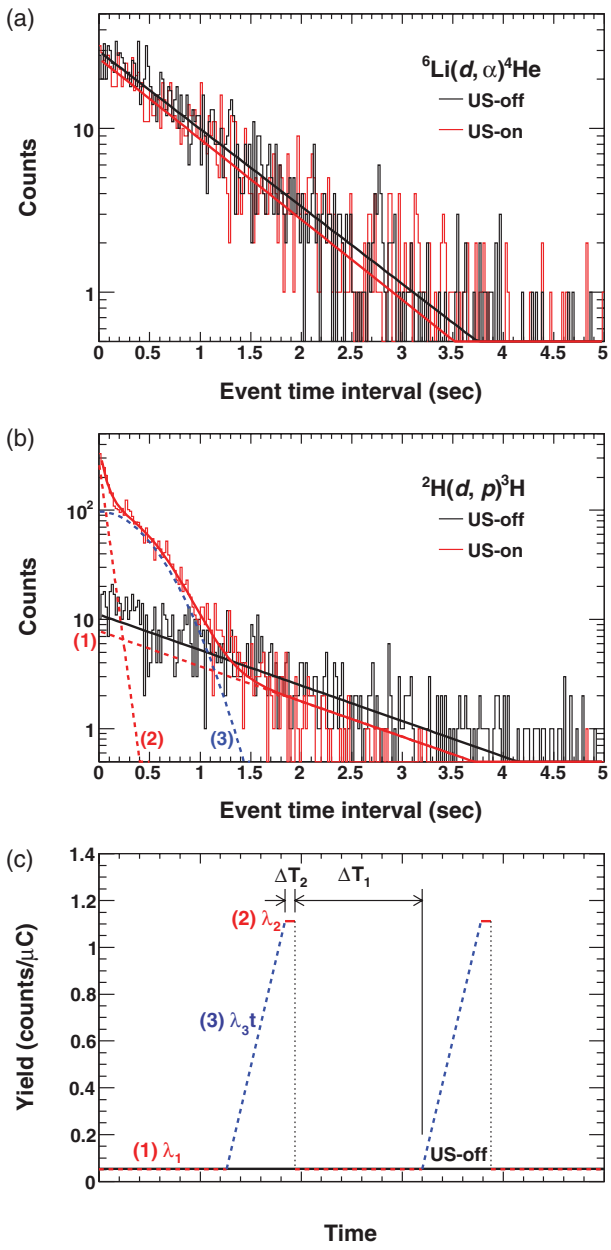

FIG. 11. (Color online) Macro time sequence information and estimated reaction rates. Data are an abstraction of those shown in Fig. 10. (a) Macro time sequence of the Li + d reaction. Histograms are fitted by Eq. (8); the reaction rate parameters λ_0 obtained in the US-off and -on states are 1.09 ± 0.04 and 1.13 ± 0.05, respectively. (b) Macro time sequence of the $d + d$ reaction. Reaction rate parameter λ_0 in the US-off state is 0.75 ± 0.05. The histogram for the US-on state has three components. The first is parallel to the histogram for the US-off state; i.e., it shows an equivalent reaction rate. The second is much steeper (i.e., represents a higher reaction rate) than the first. The first and second components are regarded as reactions in the liquid and gas phases, respectively. The histogram for the US-on state is fitted by Eq. (11); the reaction rate parameters are $\lambda_1 = 0.74 \pm 0.28$, $\lambda_2 = 15.63 \pm 1.67$, and $\lambda_3 = 5.14 \pm 0.34$. (c) Original $d + d$ reaction yield estimated from the fitting result in Fig. 11(b). The third component becomes a linear function assuming that Eq. (11) holds. In a time-average interpretation, the three components repeat sequentially.

$Z(t) = X(t) + Y(t)$ with a rate parameter $\lambda_Z = \lambda_X + \lambda_Y$. Thus, the time spectrum should contain not two but only one component having a function $y = I' e^{-(\lambda_X + \lambda_Y)t}$. Therefore, the spectrum for the US-on state in Fig. 11(b) is regarded as representing a time-dependent Poisson process. In this case, the reaction rate repeatedly alternates between λ_X and λ_Y with a certain time interval.

It is not appropriate to approximate the third component with Eq. (7) because the reaction rate is clearly time dependent. The generalized probability of the Poisson process is described as

$$P(N_t = k, t) = \frac{[\Lambda(t)]^k}{k!} e^{-\Lambda(t)}, \tag{9}$$

where $\Lambda(t)$ is the integral of the time-dependent reaction rate $\lambda(t)$,

$$\Lambda(t) = \int_0^t \lambda(x) dx. \tag{10}$$

This generalized process is known as the nonhomogeneous Poisson process (NHPP), whereas the process described by Eq. (7) is called the homogeneous Poisson process. The NHPP is applied for many continuous-time stochastic processes, for example, electrical excitation processes and neurotransmission in neuroscience [30–32].

In Fig. 11(b), the spectrum in the US-on state can be reproduced well by the following three-component function:

$$f(t) = \sum_{i=1}^{3} f_i(t) = I_1 e^{-\lambda_1 t} + I_2 e^{-\lambda_2 t} + I_3 e^{-\frac{1}{2}\lambda_3 t^2}. \tag{11}$$

The fitting result is shown by a solid line, and the components are shown by dotted lines labeled (1), (2), and (3). The calculated rate parameters are $\lambda_1 = 0.74 \pm 0.28$, $\lambda_2 = 15.63 \pm 1.67$, and $\lambda_3 = 5.14 \pm 0.34$. The third component, the last term of Eq. (11), corresponds to a time-dependent reaction rate that increases linearly with the elapsed time, i.e., $\lambda(t) = \lambda_3 t$. A simple interpretation of the total reaction rate is, for example,

$$\lambda(t) = \begin{cases} \lambda_1 & (t_{3n} < t < t_{3n+1}) \\ \lambda_3 t & (t_{3n+1} < t < t_{3n+2}) \\ \lambda_2 & (t_{3n+2} < t < t_{3n+3}) \end{cases}, \tag{12}$$

where n is natural number, including zero. The reaction occurs with two different reaction rates, λ_1 (low-rate state) and λ_2 (high-rate state) for two different time periods, $\Delta T_1 = t_{3n+1} - t_{3n}$ and $\Delta T_2 = t_{3n+3} - t_{3n+2}$, respectively. The reaction rate increases linearly with the slope of λ_3 as the reaction state changes from the low-rate to the high-rate state. The time-averaged original reaction yields can be estimated as shown in Fig. 11(c), assuming that the fitting result $\lambda_0 = 0.75$ for the US-off state is equivalent to the experimental yield of 0.053 counts/μC. The reaction is in the low-rate state alone for 65% of the measuring time and in the high-rate state or the transition state from the low-rate to the high-rate state for 35% of this run.

The existence of the high reaction rate state is clearly due to US cavitation. Because the reaction rate of the first component is almost equal to that in the US-off state, we

consider the first and second components to be caused by reactions in the liquid and gas phases, respectively. The second component, the reaction in the gas phase, maintains a high reaction rate that is more than 20 times higher than that for the first component, the reaction in the liquid phase. The third component, which corresponds to the transition state from the liquid to the gas phase, has seldom been observed before, and the time spectrum consists of only the first two components for most measurements. Note that the time variation in the reaction yield shown in Fig. 11(c) is the time-averaged value. The actual reaction rate is predicted to fluctuate locally during the measurement.

IV. ENHANCED ^{6}Li$(d,\alpha)^4$He REACTION IN LIQUID Li

As mentioned above, the effect of US waves is unstable, and the US-on/-off yield ratio is widely scattered. To investigate the reaction mechanism, we selected a relatively stable condition and measured the energy dependence of the US-on/-off yield ratio. Here we use the experimental conditions listed in Table II.

Figure 12(a) shows the energy dependence of the Li + d reaction thick target yield in the US-on state. The thick target yield Y_α can be expressed as

$$Y_\alpha(E) = 2An_d N_{\rm Li}\frac{\Omega}{4\pi}\int \sigma(E)\left(\frac{dE}{dx}\right)^{-1} dE, \qquad (13)$$

where A, n_d, and dE/dx are the coefficient, number of incident deuterons, and deuteron stopping power in Li, respectively. The detection efficiency can be regarded as unity for the SSD at the experimental reaction rate. The coefficient 2 comes from the double counting of two α particles, which cannot be differentiated from each other in the ^{6}Li$(d,\alpha_1)\alpha_2$ reaction. Equation (13) takes into account the transformation of the solid angle between the center of mass and the laboratory system. The angular distribution is negligibly small at the above-mentioned incident energies and detection angle [33]. The number density of ^{6}Li can be regarded as constant because the temperature change during the measurement, $\pm 10^\circ$C, corresponds to a 0.1% fluctuation in the density [26–28]. The proton stopping power in lithium was measured precisely by Eppacher *et al.* [34]. Because the deuteron density in liquid lithium is on the order of 0.01% of the Li density, it cannot affect the target density or stopping power [26–28]. The cross section $\sigma(E)$ is defined as in Eq. (1). The astrophysical factor $S(E)$ is an experimental value that is extrapolated from higher-energy measurements. Engstler *et al.* [33] measured the ^{6}Li$(d,\alpha)^4$He and ^{2}H$(^6$Li$,\alpha)^4$He cross sections at incident energies of $10 \leqslant E_{\rm cm} \leqslant 1450$ keV and obtained an astrophysical factor of

$$S(E) = 17.4 - 54.2E + 61.7E^2 - 23.9E^3 \ (\text{MeV b}). \qquad (14)$$

We fitted the experimental plots in Fig. 12(a) with Eq. (13) by replacing the term $\sigma(E)$ with $\sigma_0[E + U_s]$. The fitting result is shown by a solid line in Fig. 12(a). The derived screening potential of the Li + d reaction in the US-on state, within the statistical error, is $U_s = 513 \pm 54$ eV. A dotted line indicates $U_s = 0$ eV, namely the extrapolated function. Although the fitting coefficient A is expected to be 1.0, the fitting result is $A = 1.277 \pm 0.005$. In Ref. [33], the measurement is not completely absolute, but the authors normalized their experimental result by the earlier reference data. Therefore, the higher coefficient value is reasonable, and this disagreement cannot affect the obtained screening potential because the measurement and the analysis are not absolute but relative in the present experiment.

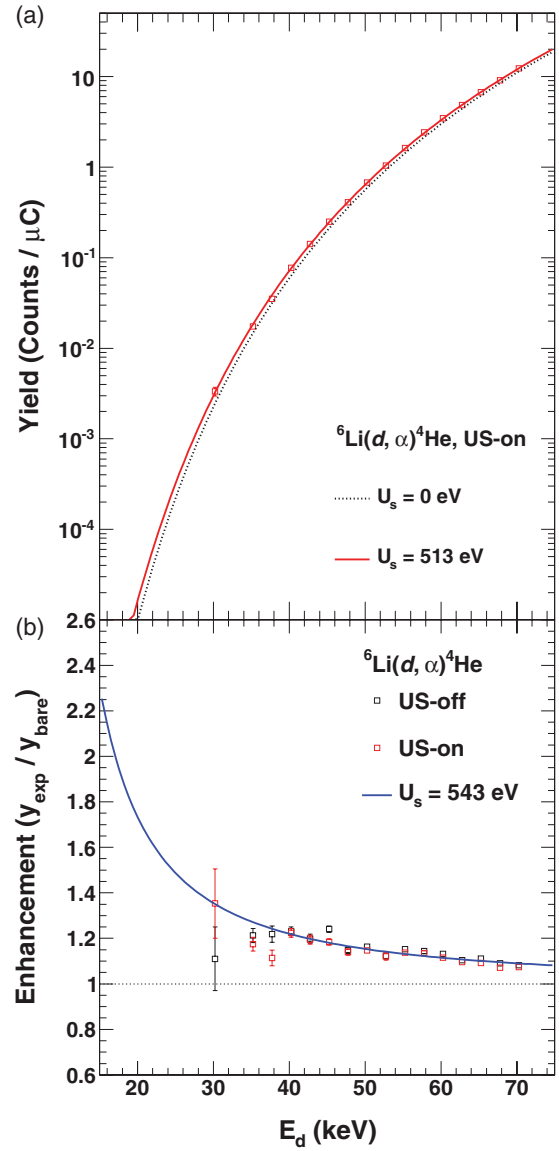

FIG. 12. (Color online) Energy dependence of thick target yield and reaction enhancement for the ^{6}Li$(d,\alpha)^4$He reaction. Vibration amplitude and temperature were $P = 1.9$ μm and $T \sim 200^\circ$C, respectively. Beam current was adjusted as the input power is equal to 500 mW. (a) Thick target yield of the Li + d reaction in the US-on state. Solid line is the best fitting result, which yields a screening potential of $U_s = 513$ eV. Dotted line corresponds to bare nuclear cross section ($U_s = 0$ eV). (b) Reaction enhancement of Li + d reaction. Experimental yields are divided by the bare yields ($U_s = 0$ eV). Solid line shows the screening potential, $U_s = 543$ eV, which is the average of the obtained potentials in both US-on and -off states.

The screening potential in the US-off state, derived by the same process, was $U_s = 574 \pm 54$ eV. Because the US effect cannot be clearly observed in the Li + d measurement, the screening potential of the Li + d reaction in liquid Li can be regarded as 543 ± 38 eV, which is the average of the values in the US-on and -off states. An enhancement factor $Y_{\rm exp}/Y_{\rm bare}$ is shown in Fig. 12(b). The deduced screening potential $U_s = 543 \pm 38$ eV predicts that the reaction rate is doubled for $E_d < 20$ keV.

In low-energy experiments, the surface condition of the target is quite important for obtaining an accurate result [11,25]. The surface layer is instantly oxidized and carbon is deposited during long-duration measurements, whereas the beam range is quite short (less than 1 μm) and the reaction occurs only in the surface region. It is difficult to keep the surface clean even in an ultrahigh vacuum [25]. In $d + d$ measurement, the target is deuteron in the solid target, and the target deuteron density is not constant. The surface condition affects the time and depth profiles of the absorbed deuterons. However, this problem in the solid target system is completely absent in the present experiment. Because the target is liquid, the contaminants, which have melting points much higher than the target temperature, float on the surface. We removed them periodically and used only the data obtained with a completely clean surface. Furthermore, the target density change is negligible. This experimental setup can measure the screening potential accurately without any type of material uncertainty.

Because the measurement and analysis are not absolute but relative, the energy dependence of each parameter provides systematic errors for the screening potential. In Eq. (13), the astrophysical factor and stopping power are energy dependent. The astrophysical factor is an experimental value determined by an absolute measurement of the nuclear fusion cross section using the equation

$$S(E) = E \exp[2\pi\eta(E)]\sigma(E). \quad (15)$$

In astrophysical factor measurement, the systematic error originates primarily in the stopping power [33]. The error in the astrophysical factor includes the stopping power error. Therefore, the error of the term $(dE/dx)^{-1}$ in the Eq. (13) was not considered to avoid counting the stopping power error twice.

Equation (15), however, is not applicable for atomic targets at lower energies because of the screening effect of valence electrons [1]. Therefore, the astrophysical factor is usually extrapolated to zero from a fitting result at higher energies. Thus, the fitting function and region have uncertainties, which increase the error. To avoid the screening effect, an indirect measurement method called the Trojan Horse method was proposed [35,36]. The astrophysical factor of the ^{6}Li(d,α)^{4}He reaction can be indirectly calculated by ^{6}Li(^{6}Li, $\alpha\alpha$)^{4}He measurement. In the Trojan Horse method, the incident ^{6}Li energy can be set high enough such that the screening effect can be ignored. Spitaleri *et al*. [37] obtained the astrophysical factor of the ^{6}Li(d,α)^{4}He reaction as

$$S(E) = 16.9 - 39.950E + 26.067E^2 \text{ (MeV b)} \quad (16)$$

by the Trojan Horse method. However, in principle, this method cannot identify the absolute value. The experimental result must be normalized by the direct measurement result at a certain energy. When the astrophysical factor in Eq. (14) is replaced by that in Eq. (16), the screening potential increases by 75 eV.

These two astrophysical factors are simple extrapolations assuming a polynomial function. The branching ratio for each channel is regarded as constant at low incident energy. The compound state ^{8}Be, however, has a wide subthreshold resonance at $E = 22.2$ MeV $(2+; 0)$ with a width of $\Gamma = 800$ keV, while the threshold is 22.28 MeV. This resonance could affect the branching ratio, which would appear to increase the yield. Czerski *et al*. revised the astrophysical factor considering the influence of the subthreshold resonance,

$$S(E) = 23.0 \exp(-4.838E + 1.3586E^2) \text{ (MeV b)}, \quad (17)$$

on the basis of direct measurement results [38]. Although the influence was estimated theoretically by the distorted-wave Born approximation method, the quantitative analysis depends on parametrizations. When the astrophysical factor in Eq. (14) is replaced with that in Eq. (17), the screening potential decreases by 149 eV.

Since Eqs. (16) and (17) have uncertainties, we adopted Eq. (14) as the most probable value. The differences in the screening potential, $^{+75}_{-149}$ eV, are considered to arise from systematic errors originating in the uncertainty in the astrophysical factor, including the stopping power error. In addition, the beam current has an uncertainty due to the sampling measurements. The maximum immediate current fluctuation is less than 10%. We estimated the systematic error originating from the beam current as $^{+8}_{-4}$ eV. The total screening potential of the ^{6}Li(d,α)^{4}He reaction in liquid Li is $U_s = 543 \pm 38$(sta.) $^{+83}_{-153}$(sys.) eV.

Engstler *et al*. measured the screening potential of the ^{6}Li(d,α)^{4}He reaction with a LiF target to be 380 ± 250 eV [33]. Although the potential of $543 \pm 38^{+8}_{-4}$ eV in the present experiment agrees with the reference value within the error, our result is slightly higher; the potential should be compared under the same astrophysical factor so the systematic error is not considered. In liquid Li, all Li atoms are dissociated as Li^{1+} and e^{1-}, which can move freely. Therefore, ionic Debye screening [12] increases the screening potential.

The total screening potential can be estimated by considering valence electrons, free electrons, and free ions, which are calculated by the adiabatic limit [39], Thomas-Fermi approximation, and Debye screening, respectively. In liquid Li, the theoretically predicted screening potential is $U_s = 639$ eV at a Li density and temperature of $N_{\rm Li} = 4.45 \times 10^{22}$ atom/cm^3 and 473 K, respectively. The experimental screening potential $543 \pm 38^{+83}_{-153}$ eV agrees with the theoretical value within the systematic error. However, the most probable value is smaller than the theoretical prediction. Although Debye screening is based on simple static conditions, the reaction enhancement depends on the dynamic mobility of ions and electrons. Because the Li^+ ion cannot exhibit full screening due to its slow mobility, the true screening potential would become lower than the static prediction.

As described above, the Li + d reaction yield was not influenced by the US effect. The Li target atom is already dissociated into ions in the liquid phase. Therefore, no additional screening effect can be generated by the transition from the liquid to the gas phase. Furthermore, the effects of the Li density and temperature changes were averaged out. The anomalously large screening potential reported in a solid metal target [40] has not been observed in liquid and gaseous metals. The obtained screening potential can be explained by the well-known ionic Debye screening model. This result implies that the anomalously large screening potential may be peculiar to the solid-state environment.

V. ENHANCED ^{2}H(d, p)^{3}H REACTION IN LIQUID Li WITH US CAVITATION

Figure 13(a) shows the energy dependence of the US-on/-off yield ratio of the ^{2}H(d,p)^{3}H reaction. The ratio tends to increase as the incident energy decreases. If the target density were increased by the US effect, the reaction yield should increase continuously; therefore, the plot in Fig. 13(a) should become flat. The data points, however, are clearly energy dependent. Therefore, the reaction is enhanced not by the change in density but by cross-section enhancement. The kinematic analysis in Fig. 8 also supports the occurrence of cross-section enhancement.

When we assume the screening effect in Li cavitation, the yield ratio can be expressed as

$$F_{\rm US}(E_d) = \frac{y_{\rm on}(E_d)}{y_{\rm off}(E_d)} \tag{18}$$

$$= B\frac{\int \sigma(E+U_s)\left(\frac{dE}{dx}\right)^{-1}dE}{\int \sigma(E)\left(\frac{dE}{dx}\right)^{-1}dE}, \tag{19}$$

where B is a coefficient. Here we adopted the astrophysical factor reported by Krauss *et al.* [41],

$$S(E) = 52.9 + 0.019E + 1.92\times10^{-3}E^2 \ (\text{keV b}). \tag{20}$$

The best fitting result, $U_s = 2086 \pm 129$ eV, is shown by a dashed line in Fig. 13(a). This potential is the largest value reported for any other host material and reaction. If we extrapolate the curve to the room temperature energy (E = 0.025 eV), the reaction rate can be calculated by replacing the cross section with $\sigma(E + U_s)$,

$$R = \frac{1}{2}N_{^2\rm H}^2\sigma v \sim 9.45\times10^{10}\left(\frac{\text{fusion}}{\text{cm}^3\text{s}}\right), \tag{21}$$

where $N_{^2\rm H}$ is assumed to be $10^{-4}\times N_{\rm Li} = 4.4\times10^{18}$ atom/cm^3. Considering the target volume and solid angle of the detector, we expect approximately 50 000 cps in this system. However, the real counting rate, a maximum of 9 cps at $E_d = 50$ keV, is much less than the predicted value. This implies that the enhancement is not caused by the screening effect, and another enhancement mechanism exists in Li acoustic cavitation.

As described in Sec. III B, the temperature in the cavity can be estimated to be on the order of 10^6 K under certain conditions. Taleyarkhan *et al.* proposed that the temperature in a certain bubble rises above 10^6 K at the instant the bubble contracts [13–15,29]. At such high temperatures, the nuclear emissions can be explained by hot fusion. We analyzed the

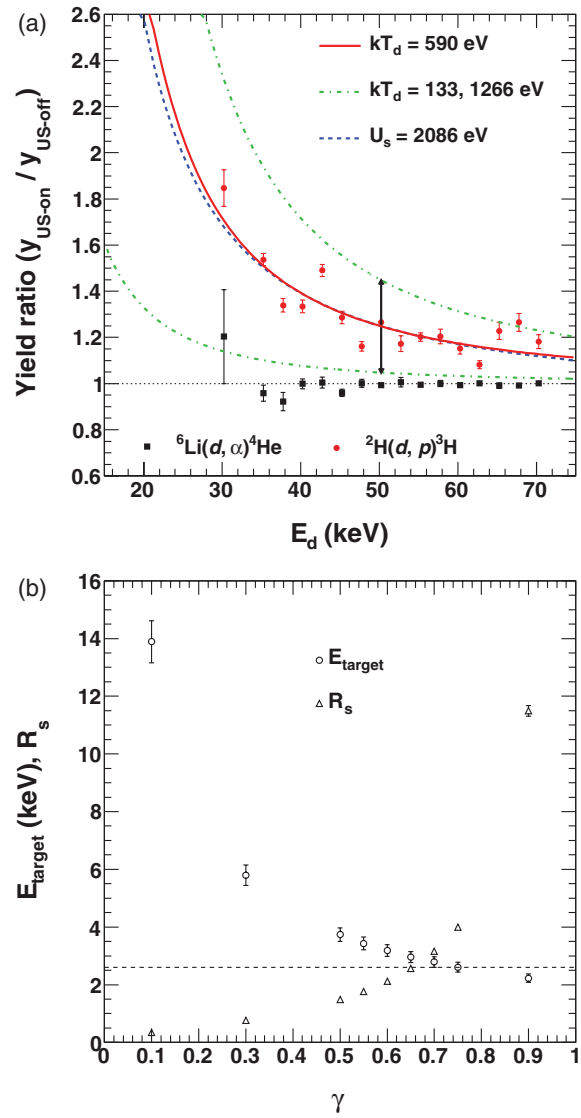

FIG. 13. (Color online) Energy dependence of US-on/-off yield ratio and gas percentage dependence of fitting results. Vibration amplitude and temperature were $P = 1.9$ μm and $T \sim 200^\circ$C, respectively. Beam current was adjusted as the input power is equal to 500 mW. (a) US-on/-off yield ratios of the ^{6}Li(d,α)^{4}He (squares) and ^{2}H(d,p)^{3}H (circles) reactions. Solid line is the best-fitting result, $kT_d = 590$ eV ($E_{\rm target} = 2959$ eV) at a gas percentage of $\gamma = 0.65$ for the $d + d$ reaction. The two long dashed-dotted lines show systematic errors, $^{+676}_{-457}$ eV, which shift the points by one standard deviation, ±0.20, at the standard energy $E_d = 50$ keV. Dashed line is the fitting result, $U_s = 2086$ eV, when the screening effect is assumed. (b) Fitting results depending on the gas percentage γ at the liquid Li surface. Circles represent target deuteron energy, $E_{\rm target}$, which is equivalent to deuteron temperature. Triangles represent theoretical gas/liquid yield ratio R_s for each γ and $E_{\rm target}$. Dashed line is an experimental value $R_s = 2.6$ obtained from the macro time sequence information. The most probable point is $\gamma = 0.65$, at which $E_{\rm target} = 2959$ eV.

data in Fig. 13(a) to evaluate the target temperature using the high-temperature model. We self-consistently evaluated three unknown factors, the temperature in the bubble, percentage of the gas phase at the surface, and deuteron density change due to acoustic cavitation, assuming the following:

(i) The Li surface is a mixture of the liquid and gas phases. The percentage of the gas phase is defined as γ ($0 < \gamma < 1$).
(ii) In the liquid phase, the screening effect is valid. According to Sec. IV, the screening potential remains constant in both US-on and -off states, and Debye screening also applies in the ^{2}H$(d,p)^3$H reaction. We assumed $U_s = 200$ eV in liquid Li, which is present at a percentage of $(1-\gamma)$.
(iii) The bubble is completely spherical.
(iv) The momentum of target deuterons in the high-temperature bubbles follows the Maxwell distribution.
(v) If the reaction occurs in the gas phase, only the high-temperature effect is important, and we ignore the screening effect. When the temperature increases, the Debye screening potential decreases according to Eq. (6), and its effect can be ignored.
(vi) Dynamic interactions between bubbles are not considered. The temperature is the same for all bubbles and all locations in each bubble.

Let $E_{\rm beam}$ and $E_{\rm target}$ be the energies of the incident deuteron and target deuteron, respectively, in the laboratory system. When we consider the collision of two particles, the energy in the center-of-mass system, $K_{\rm cm}(\theta)$, is given by

$$K_{\rm cm}(\theta) = \frac{E_{\rm beam} + E_{\rm target}}{2} - \sqrt{E_{\rm beam} E_{\rm target}}\cos\theta, \quad (22)$$

where θ is the collision angle. From Eq. (1), the cross section at low energies changes exponentially. Therefore, the cross section has a large θ dependence,

$$\sigma(\overline{K_{\rm cm}}) < \frac{\int_0^\pi \sigma[K_{\rm cm}(\theta)]\sin\theta d\theta}{\int_0^\pi \sin\theta d\theta}. \quad (23)$$

The cross section is largest when the particles collide head-on.

Under the above assumptions, the US-on/-off yield ratio can be defined as

$$F(E) = C\Bigg[(1-\gamma) + \gamma\frac{\int\int_0^\pi \sigma[K(\theta)]\left(\frac{dE}{dx}\right)^{-1}\sin\theta d\theta dE}{\int\sigma(E+U_s)\left(\frac{dE}{dx}\right)^{-1}dE\cdot\int_0^\pi\sin\theta d\theta}\Bigg], \quad (24)$$

where the coefficient C modifies the change in deuteron density in both US-on and -off states. For convenience, we ignore the transformation of the solid angle between the center of mass and laboratory systems. We fitted the data points in Fig. 13(a) with Eq. (24) in order to evaluate $E_{\rm target}$ for some given γ. The fitting results are plotted in Fig. 13(b) as circles. As the percentage of the gas phase γ decreases, the temperature in the bubble must increase in order to achieve reaction enhancement with a small number of bubbles.

Here we inferred the most probable γ using the yield ratio between the two phases. As shown in Fig. 11(b), the macro time sequence spectrum generally had two components when the $d+d$ reaction was enhanced. The third component was seldom observed; thus, it can be ignored in the following discussion. The rapid and gradual components correspond to reactions in the gas and liquid phases, respectively. First, we fitted the macro sequence spectrum of the US-off state with the function

$$y = D\exp(-\lambda_{\rm off}t) \quad (25)$$

in order to determine the reaction rate in the liquid phase, $\lambda_{\rm off}$. The term D depends on the absolute value of the deuteron density. The spectrum of the US-on state then was fitted with a two-component function,

$$y = D_{\rm off}\exp(-\lambda_{\rm off}t) + D_{\rm on}\exp(-\lambda_{\rm on}t), \quad (26)$$

where $\lambda_{\rm off}$ was fixed at the value obtained from Eq. (25). From the fitting results, the yield ratio between the two phases, R_S, can be approximated as

$$R_S = \frac{Y_{\rm gas}}{Y_{\rm liquid}} = \frac{\int_0^{10} D_{\rm on}\exp(-\lambda_{\rm on}t)dt}{\int_0^{10} D_{\rm off}\exp(-\lambda_{\rm off}t)dt}, \quad (27)$$

where the integration area is set to 10 s, which is equal to the length of the data acquisition cycle described in Sec. II B. The yield ratios were calculated for measurements made at the standard incident energy, $E_d = 50$ keV. We selected the average value, $R_S = 2.6$, as the most probable value and adopted it for $30 \leqslant E_d \leqslant 70$ keV. The error will be discussed later.

On the other hand, R_S can be expressed theoretically as

$$R_S = C\left\{\frac{\gamma\int\int_0^\pi \sigma[K(\theta)]\left(\frac{dE}{dx}\right)^{-1}\sin\theta d\theta dE}{(1-\gamma)\int\sigma(E+U_s)\left(\frac{dE}{dx}\right)^{-1}dE\int_0^\pi\sin\theta d\theta}\right\}, \quad (28)$$

where C is the same as in Eq. (24). The theoretical values for each γ are plotted as triangles in Fig. 13(b). The cross point at which the experimental value agrees with the theoretical value, $R_S = 2.6$ [dotted line in Fig. 13(b)], is the best result. The cross point appears at $\gamma = 0.65$. Consequently, we found that $E_{\rm target} = 2959 \pm 191$ eV and $C = 1.000 \pm 0.004$ was the best result, which is indicated in Fig. 13(a) by a solid line. Because the coefficient C is unity, the target density can be regarded as constant for both US-on and -off states.

The velocity of deuterium in the bubble has a Maxwell distribution,

$$f(v) = 4\pi v^2\left(\frac{m}{2\pi kT}\right)^{\frac{3}{2}}\exp\left(-\frac{mv^2}{2kT}\right), \quad (29)$$

where v and k are the velocity and the Boltzmann constant, respectively. Only a small number of deuterons distributed around the foot of the function can affect the reaction cross section. Note that $E_{\rm target}$ does not correspond to the average energy of the Maxwell distribution, $3kT/2$. Rather, $E_{\rm target}$ is defined as the energy that provides the average cross section. Therefore, $E_{\rm target}$ can be converted to the temperature by using the equation

$$\sigma\left(\frac{E_{\rm target}}{2}\right) = \int_0^\infty \sigma(v_{\rm rel})f(v)dv, \quad (30)$$

where $v_{\rm rel}$ is the relative velocity between the beam and the target particles. The target energy $E_{\rm target} = 2959 \pm 191$ eV corresponds to the temperature in the gas, $kT_d = 590 \pm 54$ eV, namely $T_d = 6.84 \times 10^6$ K. Here the order of the temperature, 10^6 K, is consistent with the value estimated from the kinematic analysis described in Sec. III B.

In the $d + d$ reaction, the US-on/-off yield ratio depends strongly on the target condition and is broadly distributed. This uncertainty exceeds all other systematic errors. Here we assume that the total systematic error is expressed by the standard deviation of the US-on/-off yield ratio at the standard beam energy $E_d = 50$ keV shown in Fig. 5, namely ± 0.20, without considering weights. The deuteron temperatures that can shift the data point by ± 0.20 at $E_d = 50$ keV are $kT_d = 133$ and 1266 eV, which are indicated by dotted lines in Fig. 13(a). Hence, we conclude that the deuteron temperature in the bubbles is $kT_d = 590 \pm 54(\text{sta.})\ ^{+676}_{-457}(\text{sys.})$.

At this temperature, the reaction rate of the background events, which are defined as reactions other than those involving the beam particles (that is, bubble fusion), can be calculated by replacing the term σv in Eq. (21) with the mean value of the Maxwell distribution $\langle \sigma v \rangle$, which is expressed as

$$\langle \sigma v \rangle = 4\pi \left(\frac{\mu}{2\pi k T_d} \right)^{\frac{3}{2}} \int_0^\infty v^3 \sigma(v) \exp\left(-\frac{\mu v^2}{2kT_{^2\rm H}} \right) dv, \quad (31)$$

$$= \left(\frac{8}{\pi \mu} \right)^{\frac{1}{2}} \left(\frac{1}{kT_d} \right)^{\frac{3}{2}} \int_0^\infty \sigma(E) E \exp\left(-\frac{E}{kT_d} \right) dE, \quad (32)$$

where μ, v, and E are the reduced mass, relative velocity, and energy in the center-of-mass system, respectively [1]. We obtain a value of $\langle \sigma v \rangle = 3.52 \times 10^{-27}$ (s/cm^3) when $kT_d = 590$ eV. Here the bubble volume is finite, and only deuterons toward the center of the bubble can contribute to the reaction. We assume that particles moving toward the spherical area whose radius is defined by $r/10$, where r is the radius of the bubble, can collide with the high-temperature particles. The reason is that the typical radius ratio is $R_0/R_m \sim 10$ in the SBSL system, where R_0 and R_m are the initial and shrunken radii, respectively [22–24,42]. The reaction rate is then estimated as $R = 1.84 \times 10^6$ fusion/(cm^3 s), which corresponds to about 0.6 cps in this experimental setup.

The estimated reaction rate describes experimental results in which significant background counts could not be detected. However, it may be possible to count the background events during long-duration measurements. Furthermore, we can expect a valid number of counts in cases of strong enhancement, such as the run shown in Fig. 7. This disagreement may be explained by a difference in the nucleus that can reduce the threshold pressure for bubble formation. The nucleus of the cavity generally consists of gas dissolved in liquid. When the liquid is irradiated by the beam, the incident particle can be regarded as an additional nucleus. In fact, the general effects of cosmic rays on the cavitation process have been considered [43]. Taleyarkhan *et al.* used neutrons or α rays as cavitation nuclei to induce bubble fusion [13–15]. They detected nuclear emission only when the liquid was irradiated by neutrons or α rays, and no significant signal was observed in the absence of radioactive rays. If the temperature in the bubble depends on the nucleus species, our experimental result that no significant events were observed in the beam-off condition is reasonable. Thus, our result agrees qualitatively with that reported by Taleyarkhan *et al.*

When the screening effect acts as the enhancement mechanism, it influences all deuterons equally; hence, the predicted reaction rate becomes much higher. In contrast, the number of deuterons that can contribute to enhancing the reaction is limited in the high-temperature bubble model due to the momentum distribution. Although the solid line (high-temperature model) is almost equivalent to the dashed line (screening model) in Fig. 13(a), the enhanced cross section drops dramatically at lower energies. Figure 14 shows the bare cross section and enhanced cross sections with $U_s = 2086$ eV and $kT_d = 590$ eV (dotted, dashed, and solid lines, respectively). Although the two enhanced lines are at almost the same level for $30 < E_d < 70$ keV, the solid line drops dramatically for $E_d < 2$ keV and, finally, becomes lower than the dashed line for $E_d < 0.5$ keV. Therefore, zero-energy reactions cannot be expected in the kinematically enhanced case.

VI. DISCUSSION

The estimated value of 10^6 K is an extremely high temperature relative to the liquid Li temperature of $T \sim 200\,^\circ$C. The acoustic cavitation process is very complex, especially in multibubble systems, and its characteristics are not necessarily clear. High pressure and high temperature are certainly achieved in the cavity. However, the reported quantitative values exhibit a broad spread because they depend on shock wave formation. Whether a shock wave forms inside a contracting bubble is one of the principal fluid dynamics questions related to acoustic cavitation. Although conditions such as bubble size, US frequency, vibration amplitude, species of liquid, and liquid temperature influence the likelihood of shock wave formation, some researchers, including Taleyarkhan, support the occurrence of shock wave formation [22,23,29,44]. The discussions in these previous studies are based on numerical simulations, and there has been no experimental evidence demonstrating shock wave formation until now. Almost all the earlier simulations assumed a single-bubble system for simplicity. In multibubble systems, such as the present experiment, the dynamics is much more complicated. Bubbles reflect the US waves, and the cycle of expansion and contraction generates a new US wave [13]. The bubble shape deviates from a sphere and the bubble diameter affects the inner temperature, which generally depends on the initial/final diameter ratio. In addition, the interaction between the bubbles, the Bjerknes force, further complicates the process [45]. Moreover, the change in the momentum of target deuterons in the bubble reflects multiple effects; thus, it is difficult to find clear signals in the micro time sequence spectra.

Here only the ^{2}H$(d,p)^3$H reaction was enhanced, and the ^{6}Li$(d,\alpha)^4$He reaction was not, although the bubbles contained primarily both Li and ^{2}H targets. This indicates that the temperature of Li did not increase significantly in the bubble. Bass *et al.* recently calculated the characteristics of a mixed-composition bubble (He and Xe) using molecular dynamics

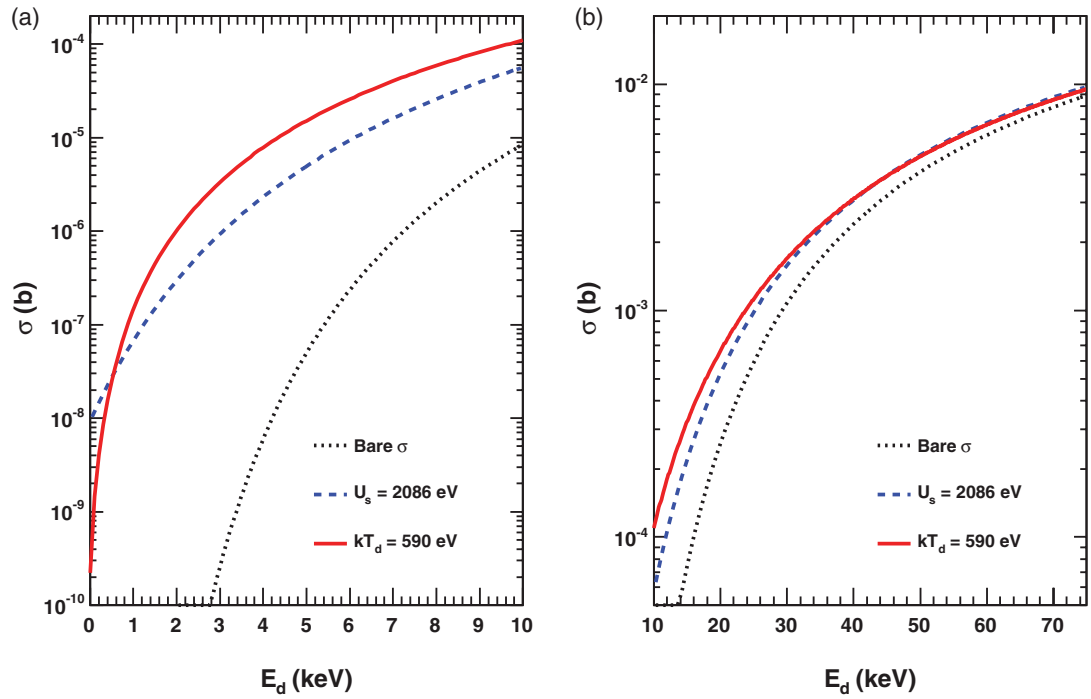

FIG. 14. (Color online) Cross section of the ^{2}H$(d,p)^3$H reaction. Horizontal axis represents incident deuteron energy in the laboratory system. Dotted, dashed, and solid lines correspond to bare, screened ($U_s = 2086$ eV), and kinematically enhanced ($kT_d = 590$ eV) cross sections, respectively. Cross section decreases dramatically at lower energies in the high-temperature model.

[46]. If a bubble includes light and heavy elements, the lighter gas is segregated and pushed by the heavier gas to compress toward the center of the bubble. The temperature and pressure of the lighter gas increase selectively, and the heavier gas remains at a relatively low temperature. The temperature in the mixed-composition bubble becomes much higher than that in a pure gas bubble due to the pressure effect. In their simulations, the lighter gas, He, reaches a maximum temperature of 10^6–10^8 K. The composition ratio plays an important role when a smaller percentage of the lighter gas achieves a higher temperature. Since the $N_{^2H}/N_{Li}$ ratio is on the order of 0.01% in our experiment, a quite high deuteron temperature can be expected. Their result agrees with our experimental result that $d + d$ fusion (involving the lighter target, ^{2}H) was accelerated, whereas Li $+ d$ fusion (involving the heavier target, Li) was not enhanced. Furthermore, the calculated temperature of the lighter gas was qualitatively equivalent to the experimental value for deuterons, $T_d = 6.84 \times 10^6$ K.

VII. CONCLUSION

We developed a new US system to produce Li acoustic cavitation in a vacuum chamber. Any impurity whose melting point was higher than the temperature of Li was removed so a completely clean surface condition could be obtained. Thus, the material uncertainties that have been noted [11] were removed, and accurate results were obtained. The ^{6}Li$(d,\alpha)^4$He and ^{2}H$(d,p)^3$H fusion reactions were measured during low-energy deuteron bombardment of a clear liquid Li target in the US-on/-off states. This is the first time that acoustic cavitation was applied to a nuclear experiment target and the first screening potential measurement in a liquid metal.

The Li $+ d$ reaction has never before been ultrasonically enhanced under all experimental conditions used in this study. An additional screening effect cannot be generated during the liquid-to-gas phase transition because the Li atoms are already dissociated into Li^+ and e^- in the liquid phase. The derived screening potential of the ^{6}Li$(d,\alpha)^4$He reaction in the liquid Li and acoustic cavitation environments is $U_s = 543 \pm 38$(sta.) $^{+83}_{-153}$(sys.) eV. This value can be explained by ionic Debye screening, which predicts that $U_s = 639$ eV under the experimental conditions. The anomalously large screening potential that has been reported for solid metal targets [40] was not observed in the liquid metal target. Therefore, the anomalous screening effect may be peculiar to the solid-state environment.

The $d + d$ reaction yield in the US-on state was always higher than that in the US-off state. Although the US effect depends strongly on the target condition, strong enhancement of the $d + d$ reaction can be induced by acoustic cavitation. Strong enhancement (US-on/-off yield ratio of more than 2.0) has seldom been observed; thus, the experimental conditions that can induce such a high yield ratio are unknown. In the most strongly enhanced case, a meaningful kinematic peak shift was observed, providing evidence of a high deuteron temperature in the cavity. The numerically simulated spectrum demonstrated good agreement with the experimental peak structure. The estimated deuteron temperature in the cavities was on the order of 10^6 K. The time correlation analyses (NHPP analyses) indicate that the reaction rate is at least time dependent.

The energy dependence of the US-on/-off yield ratio was measured under relatively stable conditions. The yield ratio exhibited an obvious energy dependence and increased at low incident energy. One possible explanation is the high deuteron temperature in the bubble. Under several assumptions, we self-consistently evaluated three unknown factors: the deuteron temperature in the bubble, percentage of the gas phase at the surface, and change in deuteron density due to acoustic cavitation. Considering the gas/liquid yield ratio obtained from the macro time sequence information, the experimental and theoretical values agree when the percentage of the gas phase at the Li surface is 65%. The estimated deuteron temperature in the bubbles is then $kT_d = 590 \pm 54(\text{sta.})\,^{+676}_{-457}(\text{sys.})$ eV, namely $T_d = 6.84 \times 10^6$ K. This result is consistent with the value estimated from the kinematic analysis.

Although the $d + d$ reaction is enhanced because of the high temperature, the yield of the $\text{Li} + d$ reaction is almost constant. This result indicates a temperature difference in the cavity: the deuteron temperature is much higher than the Li temperature. A numerical simulation [46] that calculated the molecular dynamics of bubbles consisting of a heavy and a light gas, however, agrees qualitatively with our results. An estimation of the background radiation indicates that only bubbles on which the beam particles are incident may reach such high temperatures.

The temperature in the bubbles, $kT_d = 590$ eV, is extremely high compared to the liquid Li temperature of $T \sim 200\,^{\circ}$C. Such a high temperature can never be achieved without shock wave formation in the bubble, as predicted by earlier works [22,23]. This study is the first approach for estimating the bubble temperature by applying nuclear reactions. The present techniques provided a new method for measuring temperature in an optically opaque plasma core.

Although no meaningful bubble fusion events were observed in the present study, the experimental results obviously demonstrate the possibility of strong reaction enhancement.

ACKNOWLEDGMENTS

The authors thank Kazue Matsuda for constructing the vacuum chamber in the US system. This study was partially supported by Grants-in-Aid for Scientific Research (Grants No. 19-2402, No. 19340051, and No. 23540333) from the Japan Society for the Promotion of Science. Y.T. acknowledges support as a JSPS Research Fellow.

[1] C. E. Rolfs and W. S. Rodney, *Cauldrons in the Cosmos: Nuclear Astrophysics* (University of Chicago Press, Chicago, 1988).
[2] E. E. Salpeter, Aust. J. Phys. **7**, 373 (1954).
[3] S. Ichimaru, Rev. Mod. Phys. **65**, 255 (1993).
[4] J. E. Hammel, D. W. Scudder, and J. S. Shlachter, Nucl. Instrum. Methods B **207**, 161 (1983).
[5] H. J. Assenbaum, K. Langanke, and C. Rolfs, Z. Phys. A **327**, 461 (1987).
[6] C. Rolfs and E. Somorjai, Nucl. Instrum. Methods B **99**, 297 (1995).
[7] J. Kasagi, H. Yuki, T. Baba, T. Noda, T. Ohtsuki, and A. G. Lipson, J. Phys. Soc. Jpn. **71**, 2881 (2002).
[8] F. Raiola *et al*., Eur. Phys. J. A **13**, 377 (2002).
[9] F. Raiola *et al*., Eur. Phys. J. A **19**, 283 (2004).
[10] F. Raiola *et al*., Eur. Phys. J. A **27**, 79 (2006).
[11] A. Huke, K. Czerski, P. Heide, G. Ruprecht, N. Targosz, and W. Zebrowski, Phys. Rev. C **78**, 015803 (2008).
[12] P. W. Debye and E. Hückel, Z. Phys. **24**, 185 (1923).
[13] R. P. Taleyarkhan, C. D. West, J. S. Cho, R. T. Lahey Jr., R. I. Nigmatulin, and R. C. Block, Science **295**, 1868 (2002).
[14] R. P. Taleyarkhan, J. S. Cho, C. D. West, R. T. Lahey, R. I. Nigmatulin, and R. C. Block, Phys. Rev. E **69**, 036109 (2004).
[15] R. P. Taleyarkhan, C. D. West Jr., R. T. Lahey, R. I. Nigmatulin, R. C. Block, and Y. Xu, Phys. Rev. Lett. **96**, 034301 (2006).
[16] D. Shapira and M. Saltmarsh, Phys. Rev. Lett. **89**, 104302 (2002).
[17] R. Geisler, W.-D. Schmidt-Ott, T. Kurz, and W. Lauterborn, Europhys. Lett. **66**, 435 (2004).
[18] W. C. Moss, D. B. Clarke, and D. A. Young, Science **276**, 1398 (1997).
[19] W. C. Moss, D. A. Young, J. A. Harte, J. L. Levatin, B. F. Rozsnyai, G. B. Zimmerman, and I. H. Zimmerman, Phys. Rev. E **59**, 2986 (1999).
[20] P. D. S. Burnett, D. M. Chambers, D. Heading, A. Machacek, W. C. Moss, S. Rose, M. Schnittker, R. W. Lee, P. Young, and J. S. Wark, J. Quant. Spectrosc. Radiat. Transfer **71**, 215 (2001).
[21] D. J. Flannigan and K. S. Suslick, Nature **434**, 52 (2005).
[22] C. C. Wu and P. H. Roberts, Phys. Rev. Lett. **70**, 3424 (1993).
[23] W. C. Moss, D. B. Clarke, J. W. White, and D. A. Young, Phys. Fluids **6**, 2979 (1994).
[24] D. F. Gaitan, L. A. Crum, C. C. Church, and R. A. Roy, J. Acoust. Soc. Am. **91**, 3166 (1992).
[25] A. Huke, K. Czerski, and P. Heide, Nucl. Instrum. Methods B **256**, 599 (2007).
[26] R. W. Ohse, ed. *Handbook of Thermodynamic and Transport Properties of Alkali Metals, Int. Union of Pure and Applied Chemistry Chemical Data Series No. 30*. (Blackwell Scientific, Oxford, 1985).
[27] D. W. Jeppson *et al*., Lithium Literature Review: Lithium's Properties and Interactions., HEDL-TME. 78-15 UC-20 (Hanford Engineering Development Laboratory, 1978).
[28] Y. Shimizu, A. Mizuno, T. Masaki, and T. Itami, PhysChemChemPhys **4**, 4431 (2002).
[29] R. T. Lahey Jr., R. P. Taleyarkhan, and R. I. Nigmatulin, Nucl. Eng. Des. **237**, 1571 (2007).
[30] R. W. Rodieck, N. Y. S. Kiang, and G. L. Gerstein, Biophys. J. **2**, 351 (1962).
[31] G. L. Gerstein and B. Mandelbrot, Biophys. J. **4**, 41 (1964).
[32] W. R. Softky and C. Koch, J. Neurosci. **13**, 334 (1993).
[33] S. Engstler, G. Raimann, C. Angulo, U. Greife, C. Rolfs, U. Schröder, E. Somorjai, B. Kirch, and K. Langanke, Z. Phys. A **342**, 471 (1992).
[34] Ch. Eppacher, R. Diez Muino, D. Semrad, and A. Arnau, Nucl. Instrum. Methods B **96**, 639 (1995).
[35] G. Baur, Phys. Lett. B **178**, 135 (1986).
[36] S. Typel and G. Baur, Ann. Phys. **305**, 228 (2003).

[37] C. Spitaleri *et al*., Phys. Rev. C **63**, 055801 (2001).
[38] K. Czerski, A. Huke, H. Bucka, P. Heide, G. Ruprecht, and B. Unrau, Phys. Rev. C **55**, 1517 (1997).
[39] L. Bracci, G. Fiorentini, V. S. Melezhik, G. Mezzorani, and P. Quarati, Nucl. Phys. A **513**, 316 (1990).
[40] J. Cruz *et al*., Phys. Lett. B **624**, 181 (2005).
[41] A. Krauss, H. W. Becker, H. P. Trautvetter, C. Rolfs, and K. Brand, Nucl. Phys. A **465**, 150 (1987).
[42] D. F. Gaitan and L. A. Crum, *Frontiers of Nonlinear Acoustics: Proceedings of the 12th ISNA*, edited by M. F. Hamilton and D. T. Blackstock (Elsevier Applied Science, London, New York, 1990), p. 459.
[43] D. Sette and F. Wanderlingh, Phys. Rev. **125**, 409 (1962).
[44] R. I. Nigmatulin, I. S. Akhatov, A. S. Topolnikov, R. K. Bolotnova, N. K. Vakhitova, R. T. Lahey Jr., and R. P. Taleyarkhan, Phys. Fluids **17**, 107106 (2005).
[45] R. Mettin, I. Akhatov, U. Parlitz, C. D. Ohl, and W. Lauterborn, Phys. Rev. E **56**, 2924 (1997).
[46] A. Bass, S. J. Ruuth, C. Camara, B. Merriman, and S. Putterman, Phys. Rev. Lett. **101**, 234301 (2008).